Journal of Sound and Vibration 433 (2018) 314–333

Contents lists available at ScienceDirect

Journal of Sound and Vibration

journal homepage: www.elsevier.com/locate/jsvi

Wiener Path Integral based response determination of nonlinear systems subject to non-white, non-Gaussian, and non-stationary stochastic excitation

Apostolos F. Psaros [a], Olga Brudastova [a], Giovanni Malara [b], Ioannis A. Kougioumtzoglou [a,*]

[a] Department of Civil Engineering and Engineering Mechanics, Columbia University, 500 W 120th St, New York, NY 10027, United States
[b] Department of Mechanics and Materials, "Mediterranea" University of Reggio Calabria, Feo di Vito, Reggio Calabria, 89122, Italy

ARTICLE INFO

Article history:
Received 20 December 2017
Revised 19 April 2018
Accepted 5 July 2018
Available online XXX
Handling Editor: K. Worden

Keywords:
Path integral
Non-white and non-Gaussian stochastic processes
Stochastic dynamics
Nonlinear system

ABSTRACT

The recently developed Wiener Path Integral (WPI) technique for determining the joint response probability density function of nonlinear systems subject to Gaussian white noise excitation is generalized herein to account for non-white, non-Gaussian, and non-stationary excitation processes. Specifically, modeling the excitation process as the output of a filter equation with Gaussian white noise as its input, it is possible to define an augmented response vector process to be considered in the WPI solution technique. A significant advantage relates to the fact that the technique is still applicable even for arbitrary excitation power spectrum forms. In such cases, it is shown that the use of a filter approximation facilitates the implementation of the WPI technique in a straightforward manner, without compromising its accuracy necessarily. Further, in addition to dynamical systems subject to stochastic excitation, the technique can also account for a special class of engineering mechanics problems where the media properties are modeled as stochastic fields. Several numerical examples pertaining to both single- and multi-degree-of-freedom systems are considered, including a marine structural system exposed to flow-induced non-white excitation, as well as a bending beam with a non-Gaussian and non-homogeneous Young's modulus. Comparisons with Monte Carlo simulation data demonstrate the accuracy of the technique.

1. Introduction

Uncertainty propagation in engineering mechanics and dynamics is a highly challenging problem that requires development of analytical/numerical techniques for determining the stochastic response of complex engineering systems. In this regard, although Monte Carlo simulation (MCS) has been the most versatile technique for addressing the above problem (e.g., [1,2]), it can become computationally daunting when faced with high-dimensional systems or with computing very low probability events. Thus, there is a demand for pursuing more computationally efficient methodologies. In the field of stochastic engineering dynamics, a number of alternative techniques, such as stochastic averaging (e.g., [3–5]), statistical linearization (e.g., [6–8]), as well as methodologies based on Markov approximations and related Fokker-Planck equations [9], have been developed over the

* Corresponding author.
E-mail address: ikougioum@columbia.edu (I.A. Kougioumtzoglou).

https://doi.org/10.1016/j.jsv.2018.07.013
0022-460X/

past few decades with varying degrees of accuracy.

More recently, a Wiener Path Integral (WPI) technique, whose origins can be found in theoretical physics [10], has been developed in the field of engineering dynamics for determining the response transition probability density function (PDF) of oscillators subject to Gaussian white noise excitation [11]. The technique has been generalized to account for multi-degree-of-freedom (MDOF) systems and diverse nonlinear/hysteretic system modeling [12], as well as for systems endowed with fractional derivative terms [13]. Further, the technique has been enhanced from a computational efficiency perspective by relying on its localization capabilities and invoking appropriate expansions for the response PDF [14]. In this regard, sparse PDF representations in conjunction with compressive sampling tools and group sparsity concepts have been utilized in Ref. [15] for addressing relatively high-dimensional stochastic systems. Finally, it has been shown by Kougioumtzoglou [16] that the technique can also address a special class of engineering mechanics problems where media properties are modeled as stochastic fields, while preliminary efforts on quantifying the error of the technique can be found in Ref. [17]. Nevertheless, the WPI technique has been limited so far to treating Gaussian white noise excitation processes only.

In this paper, the WPI technique is extended to account for non-white, non-Gaussian and non-stationary processes representing either the excitation of an MDOF dynamical system, or the media properties of a class of one-dimensional continuous systems. To this aim, modeling the excitation process as the output of a filter equation with Gaussian white noise as its input (e.g., [18]), it is possible to define an augmented response vector process to be considered in the WPI solution technique. A significant advantage relates to the fact that the technique is still applicable even for arbitrary excitation power spectrum forms. In such cases, it is shown that the use of a filter approximation (see also [19]) facilitates the implementation of the WPI technique in a straightforward manner. Several numerical examples pertaining to both single- and multi-degree-of-freedom systems are considered, including a marine structural system exposed to flow-induced non-white excitation, as well as a bending beam with a non-Gaussian and non-homogeneous Young's modulus. Comparisons with MCS data demonstrate the accuracy of the technique.

2. Preliminaries

2.1. Fokker-Planck equation

This section serves as a brief background on Markov processes, the associated Chapman-Kolmogorov (C-K) and Fokker-Planck (F-P) equations, as well as their relation to a corresponding stochastic differential equation (SDE).

Consider a Markov stochastic vector process, $\boldsymbol{\alpha}(t)$, where $\boldsymbol{\alpha} = [\alpha_j]_{n\times 1}$, for which the C-K equation is satisfied (e.g., [20]) for any $t_{l+1} \geq t_l \geq t_{l-1}$, i.e.,

$$p(\boldsymbol{\alpha}_{l+1}, t_{l+1} \mid \boldsymbol{\alpha}_{l-1}, t_{l-1}) = \int_{-\infty}^{\infty} p(\boldsymbol{\alpha}_{l+1}, t_{l+1} \mid \boldsymbol{\alpha}_l, t_l) p(\boldsymbol{\alpha}_l, t_l \mid \boldsymbol{\alpha}_{l-1}, t_{l-1}) \mathrm{d}\boldsymbol{\alpha}_l \tag{1}$$

where $p(\boldsymbol{\alpha}_{l+1}, t_{l+1} \mid \boldsymbol{\alpha}_{l-1}, t_{l-1})$ denotes the transition PDF of the process $\boldsymbol{\alpha}$. For a Markov process, the sample paths are continuous functions of t with probability one, if the Lindeberg condition is satisfied (e.g., [21]), namely for any $\epsilon > 0$

$$\lim_{\Delta t \to 0} \frac{1}{\Delta t} \int\limits_{|\boldsymbol{\alpha}_{l+1} - \boldsymbol{\alpha}_l| > \epsilon} p(\boldsymbol{\alpha}_{l+1}, t_{l+1} \mid \boldsymbol{\alpha}_l, t_l) \mathrm{d}\boldsymbol{\alpha}_{l+1} = 0 \tag{2}$$

where $\Delta t = t_{l+1} - t_l$. Such a process is called a diffusion process and the components of its drift vector, $\mathbf{A}(\boldsymbol{\alpha}_l, t_l) = [A_j(\boldsymbol{\alpha}_l, t_l)]_{n\times 1}$ and of its diffusion matrix $\mathbf{B}(\boldsymbol{\alpha}_l, t_l) = [B_{jk}(\boldsymbol{\alpha}_l, t_l)]_{n\times n}$ can be defined as (e.g., [22])

$$A_j(\boldsymbol{\alpha}_l, t_l) = \lim_{\Delta t \to 0} \frac{\mathbb{E}\left[\alpha_{jl+1} - \alpha_{jl}\right]}{\Delta t} \tag{3}$$

and

$$B_{jk}^2(\boldsymbol{\alpha}_l, t_l) = \lim_{\Delta t \to 0} \frac{\mathbb{E}\left[(\alpha_{jl+1} - \alpha_{jl})(\alpha_{kl+1} - \alpha_{kl})\right]}{\Delta t} \tag{4}$$

respectively. Further, employing the C-K Eq. (1) leads to the well-known F-P equation (e.g., [23,24])

$$\frac{\partial p}{\partial t} = -\sum_j \frac{\partial}{\partial \alpha_j}\left(A_j(\boldsymbol{\alpha}, t)p\right) + \frac{1}{2}\sum_{j,k} \frac{\partial}{\partial \alpha_j}\frac{\partial}{\partial \alpha_k}\left(\widetilde{B}_{jk}(\boldsymbol{\alpha}, t)p\right) \tag{5}$$

where $p = p(\boldsymbol{\alpha}_{l+1}, t_{l+1} \mid \boldsymbol{\alpha}_l, t_l)$ and $\widetilde{\mathbf{B}}(\boldsymbol{\alpha}, t) = \mathbf{B}(\boldsymbol{\alpha}, t)\mathbf{B}^T(\boldsymbol{\alpha}, t)$.

The F-P Eq. (5) is related to a first-order SDE of the form

$$\dot{\boldsymbol{\alpha}} = \mathbf{A}(\boldsymbol{\alpha}, t) + \mathbf{B}(\boldsymbol{\alpha}, t)\boldsymbol{\eta}(t) \tag{6}$$

where the dot above a variable denotes differentiation with respect to time t and $\boldsymbol{\eta}(t)$ is a zero-mean and delta-correlated process of intensity one; i.e., $\mathbb{E}\left[\eta_j(t)\right] = 0$ and $\mathbb{E}\left[\eta_j(t_l)\eta_k(t_{l+1})\right] = \delta_{jk}\delta(t_l - t_{l+1})$, for any $j, k \in \{1, \ldots, n\}$, where δ_{jk} is the Kronecker delta, and $\delta(t)$ is the Dirac delta function.

2.2. WPI formulation

In the limit $\Delta t \to 0$ the transition PDF has been shown to admit a Gaussian distribution (e.g., [22,25]) of the form

$$p(\boldsymbol{\alpha}_{l+1}, t_{l+1} \mid \boldsymbol{\alpha}_l, t_l) = \left[\sqrt{(2\pi\Delta t)^n \det\left[\widetilde{\mathbf{B}}(\boldsymbol{\alpha}_l, t_l)\right]}\right]^{-1} \times \dots$$
$$\exp\left(-\frac{1}{2}\frac{[\boldsymbol{\alpha}_{l+1} - \boldsymbol{\alpha}_l - \Delta t\mathbf{A}(\boldsymbol{\alpha}_l, t_l)]^T\left[\widetilde{\mathbf{B}}(\boldsymbol{\alpha}_l, t_l)\right]^{-1}[\boldsymbol{\alpha}_{l+1} - \boldsymbol{\alpha}_l - \Delta t\mathbf{A}(\boldsymbol{\alpha}_l, t_l)]}{\Delta t}\right) \tag{7}$$

Note here that the choice of Eq. (7) is not restrictive, and non-Gaussian distributions can also be employed (e.g., [26,27]). In fact, Eq. (7), in conjunction with the C-K Eq. (1), has been the starting point of alternative purely numerical schemes in the literature (typically referred to as numerical path integral schemes) for propagating the response PDF in short time steps [28–31]. Although these schemes have proven to be highly accurate as the only approximation relates to the discretization of the C-K Eq. (1), they can be computationally demanding. This is due to the fact that numerical computation of a multi-dimensional convolution integral is required for each and every time step, while the time step has to be kept short. In Eq. (7) it is assumed that $\widetilde{\mathbf{B}}$ is a non-singular matrix and its inverse exists.

Further, the probability that $\boldsymbol{\alpha}$ follows a specific path, $\boldsymbol{\alpha}(t)$, can be construed as the probability of a compound event. In particular, it is expressed (e.g., [10,25]) as the product of probabilities of the form of Eq. (7), i.e.,

$$\mathrm{P}[\boldsymbol{\alpha}(t)] = \lim_{\substack{\Delta t \to 0 \\ N \to \infty}} \left\{\left[\prod_{l=0}^{N-1}\left(\left[\sqrt{(2\pi\Delta t)^n \det\left[\widetilde{\mathbf{B}}(\boldsymbol{\alpha}_l, t_l)\right]}\right]^{-1}\prod_{j=1}^{n}\mathrm{d}\alpha_{jl}\right)\right] \times \dots\right.$$
$$\left.\exp\left(-\sum_{l=0}^{N-1}\frac{1}{2}\frac{\left[\boldsymbol{\alpha}_{l+1} - \boldsymbol{\alpha}_l - \Delta t\mathbf{A}(\boldsymbol{\alpha}_l, t_l)\right]^T\left[\widetilde{\mathbf{B}}(\boldsymbol{\alpha}_l, t_l)\right]^{-1}\left[\boldsymbol{\alpha}_{l+1} - \boldsymbol{\alpha}_l - \Delta t\mathbf{A}(\boldsymbol{\alpha}_l, t_l)\right]}{\Delta t}\right)\right\} \tag{8}$$

where the time has been discretized into N points, Δt apart, and the path $\boldsymbol{\alpha}(t)$ is represented by its values $\boldsymbol{\alpha}_l$ at the discrete time points t_l, for $l \in \{0, \dots, N-1\}$. Also, $\mathrm{d}\alpha_{jl}$ denote the (infinite in number) infinitesimal "gates" through which the path propagates. Loosely speaking, Eq. (8) represents the probability of the process to propagate through the infinitesimally thin tube surrounding $\boldsymbol{\alpha}(t)$. Note that if the diffusion matrix, $\mathbf{B}(\boldsymbol{\alpha}, t)$, is diagonal, Eq. (8) can be written in the compact form [10]

$$\mathrm{P}[\boldsymbol{\alpha}(t)] = \exp\left(-\int_{t_i}^{t_f}\frac{1}{2}\sum_{j=1}^{n}\frac{[\dot{\alpha}_j - A_j(\boldsymbol{\alpha}, t)]^2}{\widetilde{B}_{jj}(\boldsymbol{\alpha}, t)}\mathrm{d}t\right)\prod_{j=1}^{n}\prod_{t=t_i}^{t_f}\frac{\mathrm{d}\alpha_j(t)}{\sqrt{2\pi\widetilde{B}_{jj}(\boldsymbol{\alpha}, t)\mathrm{d}t}} \tag{9}$$

Overall, the total probability that $\boldsymbol{\alpha}$ will start from $\boldsymbol{\alpha}_i$ at time t_i and end up at $\boldsymbol{\alpha}_f$ at time t_f takes the form of a functional integral, which "sums up" the respective probabilities of each and every path that the process can possibly follow (see, e.g., [10,32]). Next, denoting the set of all paths with initial state $\boldsymbol{\alpha}_i$ at time t_i and final state $\boldsymbol{\alpha}_f$ at time t_f by $C\{\boldsymbol{\alpha}_i, t_i; \boldsymbol{\alpha}_f, t_f\}$, the transition PDF takes the form

$$p(\boldsymbol{\alpha}_f, t_f \mid \boldsymbol{\alpha}_i, t_i) = \int_{C\{\boldsymbol{\alpha}_i, t_i; \boldsymbol{\alpha}_f, t_f\}}\exp\left(-\int_{t_i}^{t_f}L[\boldsymbol{\alpha}, \dot{\boldsymbol{\alpha}}]\,\mathrm{d}t\right)\prod_{j=1}^{n}\mathcal{D}[\alpha_j(t)] \tag{10}$$

where $L[\boldsymbol{\alpha}, \dot{\boldsymbol{\alpha}}]$ denotes the Lagrangian functional of the system and is expressed as

$$L[\boldsymbol{\alpha}, \dot{\boldsymbol{\alpha}}] = \frac{1}{2}\sum_{j=1}^{n}\frac{[\dot{\alpha}_j - A_j(\boldsymbol{\alpha}, t)]^2}{\widetilde{B}_{jj}(\boldsymbol{\alpha}, t)} \tag{11}$$

and $\mathcal{D}[\alpha_j(t)]$, for $j \in \{1, \dots, n\}$, is a functional measure given as

$$\mathcal{D}[\alpha_j(t)] = \prod_{t=t_i}^{t_f}\frac{\mathrm{d}\alpha_j(t)}{\sqrt{2\pi\widetilde{B}_{jj}(\boldsymbol{\alpha}, t)\mathrm{d}t}} \tag{12}$$

Based on the aforementioned concepts, Kougioumtzoglou and coworkers developed recently a WPI technique for determining the response transition PDF of stochastically excited MDOF systems [12,14]. Although the technique has proven to be versatile in addressing various system nonlinearity types and even fractional derivative terms [13], its applicability has been limited so far to Gaussian white noise excitation processes only. In the following section, the WPI technique is generalized to account for (non-stationary) non-Gaussian and non-white processes as well.

3. Mathematical formulation

3.1. WPI technique generalization: non-white and non-Gaussian excitation process

3.1.1. Theoretical formulation

Consider the m-degree-of-freedom nonlinear system

$$\mathbf{M}\ddot{\mathbf{x}} + \mathbf{C}\dot{\mathbf{x}} + \mathbf{K}\mathbf{x} + \mathbf{g}(\mathbf{x}, \dot{\mathbf{x}}) = \boldsymbol{\xi}(t) \tag{13}$$

where $\mathbf{x}(t) = [x_1, \ldots, x_m]^T$ is the displacement vector process; $\mathbf{M}, \mathbf{C}, \mathbf{K}$ represent the $m \times m$ mass, damping and stiffness matrices, respectively, and $\mathbf{g}(\mathbf{x}, \dot{\mathbf{x}})$ denotes an arbitrary nonlinear vector function. $\boldsymbol{\xi}(t)$ is a non-white and non-Gaussian in general excitation stochastic process, which is modeled as the response of the nonlinear "filter" equation (e.g., [6])

$$\mathbf{P}\ddot{\boldsymbol{\xi}} + \mathbf{Q}\dot{\boldsymbol{\xi}} + \mathbf{R}\boldsymbol{\xi} + \mathbf{u}(\boldsymbol{\xi}, \dot{\boldsymbol{\xi}}) = \mathbf{w}(t) \tag{14}$$

where $\mathbf{P}, \mathbf{Q}, \mathbf{R}$ denote coefficient matrices; $\mathbf{u}(\boldsymbol{\xi}, \dot{\boldsymbol{\xi}})$ is an arbitrary nonlinear vector function; and $\mathbf{w}(t) = [w_1, \ldots, w_m]^T$ is a white noise stochastic vector process with the power spectrum matrix

$$\mathbf{S}_{\mathbf{w}} = \begin{bmatrix} S_0 & \ldots & 0 \\ \vdots & \ddots & \vdots \\ 0 & \ldots & S_0 \end{bmatrix} \tag{15}$$

Note that various non-white excitation processes, commonly utilized in engineering dynamics (e.g., the Kanai-Tajimi excitation process in earthquake engineering [33,34]), can be described by the filter Eq. (14). In fact, Eq. (14) can be construed as the time-domain representation of such excitation processes that are typically described in the frequency domain via power spectra [35]. In addition, even in cases where the excitation power spectrum cannot be represented in the time domain as the response of a filter, it has been shown [18,19] that a filter approximation of the form of Eq. (14) exhibits, in general, satisfactory accuracy for practical applications. Further, Eq. (14) can also account for non-Gaussian excitation modeling via the nonlinear function $\mathbf{u}(\boldsymbol{\xi}, \dot{\boldsymbol{\xi}})$.

Next, differentiating Eq. (13) and substituting into Eq. (14) yields the fourth-order SDE

$$\boldsymbol{\Lambda}_4\mathbf{x}^{(4)} + \boldsymbol{\Lambda}_3\mathbf{x}^{(3)} + \boldsymbol{\Lambda}_2\ddot{\mathbf{x}} + \boldsymbol{\Lambda}_1\dot{\mathbf{x}} + \boldsymbol{\Lambda}_0\mathbf{x} + \mathbf{h}(\mathbf{x}, \dot{\mathbf{x}}, \ddot{\mathbf{x}}, \mathbf{x}^{(3)}) = \mathbf{w}(t) \tag{16}$$

where

$$\begin{cases} \boldsymbol{\Lambda}_4 = \mathbf{PM} \\ \boldsymbol{\Lambda}_3 = \mathbf{PC} + \mathbf{QM} \\ \boldsymbol{\Lambda}_2 = \mathbf{PK} + \mathbf{QC} + \mathbf{RM} \\ \boldsymbol{\Lambda}_1 = \mathbf{QK} + \mathbf{RC} \\ \boldsymbol{\Lambda}_0 = \mathbf{RK} \end{cases} \tag{17}$$

and

$$\mathbf{h}(\mathbf{x}, \dot{\mathbf{x}}, \ddot{\mathbf{x}}, \mathbf{x}^{(3)}) = \mathbf{P}\ddot{\mathbf{g}}(\mathbf{x}, \dot{\mathbf{x}}) + \mathbf{Q}\dot{\mathbf{g}}(\mathbf{x}, \dot{\mathbf{x}}) + \mathbf{R}\mathbf{g}(\mathbf{x}, \dot{\mathbf{x}}) + \mathbf{u}(\mathbf{x}, \dot{\mathbf{x}}, \ddot{\mathbf{x}}, \mathbf{x}^{(3)}) \tag{18}$$

Eq. (16) can be cast in a state variable formulation [25,36,37], and take the form of Eq. (6), where

$$\boldsymbol{\alpha} = [\mathbf{x}, \mathbf{y}_1, \mathbf{y}_2, \mathbf{y}_3]^T \tag{19}$$

$$\mathbf{A}(\boldsymbol{\alpha}, t) = \begin{bmatrix} \mathbf{y}_1 \\ \mathbf{y}_2 \\ \mathbf{y}_3 \\ \boldsymbol{\Lambda}_4^{-1}\left(-\boldsymbol{\Lambda}_3\mathbf{y}_3 - \boldsymbol{\Lambda}_2\mathbf{y}_2 - \boldsymbol{\Lambda}_1\mathbf{y}_1 - \boldsymbol{\Lambda}_0\mathbf{x} - \mathbf{h}(\mathbf{x}, \mathbf{y}_1, \mathbf{y}_2, \mathbf{y}_3)\right) \end{bmatrix} \tag{20}$$

and

$$\mathbf{B}(\boldsymbol{\alpha}, t) = \begin{bmatrix} \mathbf{0}_{3m\times 3m} & \mathbf{0}_{3m\times m} \\ \mathbf{0}_{m\times 3m} & \sqrt{2\pi}\boldsymbol{\Lambda}_4^{-1}\mathbf{S}_{\mathbf{w}}^{1/2} \end{bmatrix} \tag{21}$$

In this regard, the m-dimensional fourth-order SDE of Eq. (16) becomes a $4m$-dimensional first-order SDE for the process $\boldsymbol{\alpha} = [\mathbf{x}, \mathbf{y}_1, \mathbf{y}_2, \mathbf{y}_3]^T$.

Note, however, that the diffusion matrix $\mathbf{B}(\boldsymbol{\alpha}, t)$ (as well as $\widetilde{\mathbf{B}}(\boldsymbol{\alpha}, t) = \mathbf{B}(\boldsymbol{\alpha}, t)\mathbf{B}^T(\boldsymbol{\alpha}, t)$) in Eq. (21) is singular, and thus, Eq. (10) cannot be used directly. In fact, the challenge of accounting for singular diffusion matrices in conjunction with path integral formulations has received considerable attention in the literature (see Refs. [36–44]). In the ensuing analysis, the singularity of matrix $\mathbf{B}(\boldsymbol{\alpha}, t)$ is bypassed by employing delta-functionals in the path integral formulation [10,45], which enforce the compatibility equations ($\dot{\mathbf{x}} = \mathbf{y}_1$; $\dot{\mathbf{y}}_1 = \mathbf{y}_2$; and $\dot{\mathbf{y}}_2 = \mathbf{y}_3$). In this respect, the transition PDF of $\boldsymbol{\alpha} = [\mathbf{x}, \mathbf{y}_1, \mathbf{y}_2, \mathbf{y}_3]^T$ can be written as [10]

$$p(\boldsymbol{\alpha}_f, t_f \mid \boldsymbol{\alpha}_i, t_i) = \int_{C\{\boldsymbol{\alpha}_f, t_f; \boldsymbol{\alpha}_i, t_i\}} \exp\left(-\int_{t_i}^{t_f} \frac{1}{2}\mathbf{S}^T \widetilde{\mathbf{B}}_{ns}^{-1}\mathbf{S}\, \mathrm{d}t\right) \times \ldots$$
$$\delta[\dot{\mathbf{y}}_2 - \mathbf{y}_3]\delta[\dot{\mathbf{y}}_1 - \mathbf{y}_2]\delta[\dot{\mathbf{x}} - \mathbf{y}_1]\mathcal{D}[\mathbf{x}(t)]\mathcal{D}[\mathbf{y}_1(t)]\mathcal{D}[\mathbf{y}_2(t)]\mathcal{D}[\mathbf{y}_3(t)] \tag{22}$$

where $\mathbf{S} = \boldsymbol{\Lambda}_4\dot{\mathbf{y}}_3 + \boldsymbol{\Lambda}_3\mathbf{y}_3 + \boldsymbol{\Lambda}_2\mathbf{y}_2 + \boldsymbol{\Lambda}_1\mathbf{y}_1 + \boldsymbol{\Lambda}_0\mathbf{x} + \mathbf{h}(\mathbf{x}, \mathbf{y}_1, \mathbf{y}_2, \mathbf{y}_3)$ and

$$\widetilde{\mathbf{B}}_{ns} = \begin{bmatrix} 2\pi S_0 & \ldots & 0 \\ \vdots & \ddots & \vdots \\ 0 & \ldots & 2\pi S_0 \end{bmatrix} \tag{23}$$

Following integration over paths $\mathbf{y}_1(t)$, $\mathbf{y}_2(t)$ and $\mathbf{y}_3(t)$ [45], Eq. (22) becomes

$$p\left(\mathbf{x}_f, \dot{\mathbf{x}}_f, \ddot{\mathbf{x}}_f, \mathbf{x}_f^{(3)}, t_f \mid \mathbf{x}_i, \dot{\mathbf{x}}_i, \ddot{\mathbf{x}}_i, \mathbf{x}_i^{(3)}, t_i\right) = \int_{C\{\mathbf{x}_i, \dot{\mathbf{x}}_i, \ddot{\mathbf{x}}_i, \mathbf{x}_i^{(3)}, t_i; \mathbf{x}_f, \dot{\mathbf{x}}_f, \ddot{\mathbf{x}}_f, \mathbf{x}_f^{(3)}, t_f\}} \exp\left(-\int_{t_i}^{t_f} L\left[\mathbf{x}, \dot{\mathbf{x}}, \ddot{\mathbf{x}}, \mathbf{x}^{(3)}, \mathbf{x}^{(4)}\right] \mathrm{d}t\right)\mathcal{D}[\mathbf{x}(t)] \tag{24}$$

where the Lagrangian $L\left[\mathbf{x}, \dot{\mathbf{x}}, \ddot{\mathbf{x}}, \mathbf{x}^{(3)}, \mathbf{x}^{(4)}\right]$ is given by

$$L\left[\mathbf{x}, \dot{\mathbf{x}}, \ddot{\mathbf{x}}, \mathbf{x}^{(3)}, \mathbf{x}^{(4)}\right] = \frac{1}{2}\left[\boldsymbol{\Lambda}_4\mathbf{x}^{(4)} + \boldsymbol{\Lambda}_3\mathbf{x}^{(3)} + \boldsymbol{\Lambda}_2\ddot{\mathbf{x}} + \boldsymbol{\Lambda}_1\dot{\mathbf{x}} + \boldsymbol{\Lambda}_0\mathbf{x} + \mathbf{h}\left(\mathbf{x}, \dot{\mathbf{x}}, \ddot{\mathbf{x}}, \mathbf{x}^{(3)}\right)\right]^T \times \ldots$$
$$\widetilde{\mathbf{B}}_{ns}^{-1}\left[\boldsymbol{\Lambda}_4\mathbf{x}^{(4)} + \boldsymbol{\Lambda}_3\mathbf{x}^{(3)} + \boldsymbol{\Lambda}_2\ddot{\mathbf{x}} + \boldsymbol{\Lambda}_1\dot{\mathbf{x}} + \boldsymbol{\Lambda}_0\mathbf{x} + \mathbf{h}\left(\mathbf{x}, \dot{\mathbf{x}}, \ddot{\mathbf{x}}, \mathbf{x}^{(3)}\right)\right] \tag{25}$$

The formal expression of the path integral in Eq. (24) is of little practical use as its analytical or numerical evaluation is highly challenging [10]. Therefore, an approximate approach is required. In this regard, the "most probable path" approach (e.g., [10,11]) is employed, according to which the largest contribution to the transition PDF of Eq. (24) comes from the path $\mathbf{x}_c(t)$ that minimizes the integral inside the exponential. According to calculus of variations (e.g., [46]), $\mathbf{x}_c(t)$ satisfies the extremality condition

$$\delta\int_{t_i}^{t_f} L\left[\mathbf{x}_c, \dot{\mathbf{x}}_c, \ddot{\mathbf{x}}_c, \mathbf{x}_c^{(3)}, \mathbf{x}_c^{(4)}\right] \mathrm{d}t = 0 \tag{26}$$

which yields the system of Euler-Lagrange (E-L) equations

$$\begin{gathered} \frac{\partial L}{\partial x_{c,1}} - \frac{\partial}{\partial t}\frac{\partial L}{\partial \dot{x}_{c,1}} + \frac{\partial^2}{\partial t^2}\frac{\partial L}{\partial \ddot{x}_{c,1}} - \frac{\partial^3}{\partial t^3}\frac{\partial L}{\partial x_{c,1}^{(3)}} + \frac{\partial^4}{\partial t^4}\frac{\partial L}{\partial x_{c,1}^{(4)}} = 0 \\ \vdots \\ \frac{\partial L}{\partial x_{c,m}} - \frac{\partial}{\partial t}\frac{\partial L}{\partial \dot{x}_{c,m}} + \frac{\partial^2}{\partial t^2}\frac{\partial L}{\partial \ddot{x}_{c,m}} - \frac{\partial^3}{\partial t^3}\frac{\partial L}{\partial x_{c,m}^{(3)}} + \frac{\partial^4}{\partial t^4}\frac{\partial L}{\partial x_{c,m}^{(4)}} = 0 \end{gathered} \tag{27}$$

together with $8 \times m$ boundary conditions

$$\begin{array}{llll} x_{c,1}(t_i) = x_{1,i}, & \dot{x}_{c,1}(t_i) = \dot{x}_{1,i}, & x_{c,1}(t_f) = x_{1,f}, & \dot{x}_{c,1}(t_f) = \dot{x}_{1,f} \\ \ddot{x}_{c,1}(t_i) = \ddot{x}_{1,i}, & x_{c,1}^{(3)}(t_i) = x_{1,i}^{(3)}, & \ddot{x}_{c,1}(t_f) = \ddot{x}_{1,f}, & x_{c,1}^{(3)}(t_f) = x_{1,f}^{(3)} \\ & & \vdots & \\ x_{c,m}(t_i) = x_{m,i}, & \dot{x}_{c,m}(t_i) = \dot{x}_{m,i}, & x_{c,m}(t_f) = x_{m,f}, & \dot{x}_{c,m}(t_f) = \dot{x}_{m,f} \\ \ddot{x}_{c,m}(t_i) = \ddot{x}_{m,i}, & x_{c,m}^{(3)}(t_i) = x_{m,i}^{(3)}, & \ddot{x}_{c,m}(t_f) = \ddot{x}_{m,f}, & x_{c,m}^{(3)}(t_f) = x_{m,f}^{(3)} \end{array} \tag{28}$$

Next, solving the boundary value problem (BVP) of Eqs. (27) and (28) (e.g., [47,48]) yields the most probable path $\mathbf{x}_c(t)$ (m-dimensional), and the transition PDF from the initial state $\{\mathbf{x}_i, \dot{\mathbf{x}}_i, \ddot{\mathbf{x}}_i, \mathbf{x}_i^{(3)}, t_i\}$ to the final state $\{\mathbf{x}_f, \dot{\mathbf{x}}_f, \ddot{\mathbf{x}}_f, \mathbf{x}_f^{(3)}, t_f\}$ is determined as

$$p\left(\mathbf{x}_f, \dot{\mathbf{x}}_f, \ddot{\mathbf{x}}_f, \mathbf{x}_f^{(3)}, t_f \mid \mathbf{x}_i, \dot{\mathbf{x}}_i, \ddot{\mathbf{x}}_i, \mathbf{x}_i^{(3)}, t_i\right) = C\exp\left(-\int_{t_i}^{t_f} L\left[\mathbf{x}_c, \dot{\mathbf{x}}_c, \ddot{\mathbf{x}}_c, \mathbf{x}_c^{(3)}, \mathbf{x}_c^{(4)}\right] \mathrm{d}t\right) \tag{29}$$

where the normalization constant C is evaluated based on the condition

$$\int_{-\infty}^{\infty} \cdots \int_{-\infty}^{\infty} p\left(\mathbf{x}_f, \dot{\mathbf{x}}_f, \ddot{\mathbf{x}}_f, \mathbf{x}_f^{(3)}, t_f \mid \mathbf{x}_i, \dot{\mathbf{x}}_i, \ddot{\mathbf{x}}_i, \mathbf{x}_i^{(3)}, t_i\right) \mathrm{d}\mathbf{x}_f \ldots \mathrm{d}\mathbf{x}_f^{(3)} = 1 \tag{30}$$

3.1.2. Computational aspects

This section is concerned with the numerical implementation of the WPI technique as developed in Section 3.1.1. In this regard, note that one point of the PDF is computed by solving one BVP of the form of Eqs. (27) and (28). According to a brute force implementation of the technique, for a given time instant t_f an effective domain of boundary values is considered for the PDF. Following the discretization of the effective domain into N_s points $\left(\mathbf{x}_f, \dot{\mathbf{x}}_f, \ddot{\mathbf{x}}_f, \mathbf{x}_f^{(3)}\right)$ in each dimension, the response PDF is determined for each point of the mesh. Specifically, for an m-DOF system, the number of BVPs required to be solved is $N_s^{4\ \mathrm{m}}$. It is clear that the computational cost becomes prohibitive for relatively high-dimensional MDOF systems, however, efficient implementations, such as the ones developed by Kougioumtzoglou et al. [14] and Psaros et al. [15], can be utilized in conjunction with the herein generalized WPI technique. Specifically, according to [14], utilizing a polynomial expansion for the joint response PDF yields a number of BVPs to be solved equal to the number of the expansion coefficients. This implementation has been shown to follow approximately a power-law function of the form $\sim (4\ \mathrm{m})^{d_p}/d_p!$ (where d_p is the degree of the polynomial), which, depending on the value of m, can be orders of magnitude smaller than N_s^{4m} [14]. In addition, if sparse PDF representations in conjunction with compressive sampling tools and group sparsity concepts are utilized, the required number of BVPs to be solved can be reduced even further [15].

3.2. WPI technique generalization: non-stationary excitation process

3.2.1. Theoretical formulation

It can be readily seen that Section 3.1 refers to stochastic modeling that accounts for the transient phase of the excitation filter in Eq. (14). In other words, the non-white excitation process $\boldsymbol{\xi}(t)$ in Eq. (13) is an overall non-stationary process since the WPI technique as developed in Section 3.1 accounts also for its transient phase though Eq. (14). However, in many engineering dynamics applications the excitation model is provided in the form of a (time-modulated) power spectrum [6,35]

$$\mathbf{S_f}(\omega, t) = \mathbf{D}(t)\mathbf{S}_{\xi_s}(\omega)\mathbf{D}^T(t) \tag{31}$$

corresponding to the (non-stationary) stochastic process

$$\mathbf{f}(t) = \mathbf{D}(t)\boldsymbol{\xi}_s(t) \tag{32}$$

where $\mathbf{D}(t) = [D_{jk}(t)]_{m\times m}$ is a matrix of deterministic time-modulating functions. Note that in Eqs. (31) and (32) $\boldsymbol{\xi}_s(t)$ represents the stationary output of Eq. (14); that is, the output of Eq. (14) after its transient phase has died out, and $\boldsymbol{\xi}(t)$ has reached its stationary phase. Clearly, a modification in the implementation of the WPI technique of Section 3.1 is required to account for stochastic excitation modeling via Eqs. (31) and (32).

In particular, Eq. (13) takes the form

$$\mathbf{M}\ddot{\mathbf{x}} + \mathbf{C}\dot{\mathbf{x}} + \mathbf{K}\mathbf{x} + \mathbf{g}(\mathbf{x}, \dot{\mathbf{x}}) = \mathbf{f}(t) \tag{33}$$

while considering Eq. (32) with $D_{jk}(t) \neq 0, \forall j, k \in \{1, \ldots, m\}$, yields

$$\boldsymbol{\xi}_s(t) = \mathbf{D}^{-1}(t)\mathbf{f}(t) \tag{34}$$

$$\dot{\boldsymbol{\xi}}_s(t) = \mathbf{D}^{-1}(t)\left[\dot{\mathbf{f}}(t) - \dot{\mathbf{D}}(t)\boldsymbol{\xi}_s(t)\right] \tag{35}$$

$$\ddot{\boldsymbol{\xi}}_s(t) = \mathbf{D}^{-1}(t)\left[\ddot{\mathbf{f}}(t) - \ddot{\mathbf{D}}(t)\boldsymbol{\xi}_s(t) - 2\dot{\mathbf{D}}(t)\dot{\boldsymbol{\xi}}_s(t)\right] \tag{36}$$

Next, substituting Eqs. (33)–(36) into Eq. (14), an SDE similar to the one described by Eq. (16) is obtained, with

$$\begin{cases} \mathbf{\Lambda}_4 = \mathbf{P}\mathbf{D}^{-1}\mathbf{M} \\ \mathbf{\Lambda}_3 = \mathbf{P}\mathbf{D}^{-1}\left[-2\dot{\mathbf{D}}\mathbf{D}^{-1}\mathbf{M} + \mathbf{C}\right] + \mathbf{Q}\mathbf{D}^{-1}\mathbf{M} \\ \mathbf{\Lambda}_2 = \mathbf{P}\mathbf{D}^{-1}\left[\left(2\dot{\mathbf{D}}\mathbf{D}^{-1}\dot{\mathbf{D}}\mathbf{D}^{-1} - \ddot{\mathbf{D}}\mathbf{D}^{-1}\right)\mathbf{M} - 2\dot{\mathbf{D}}\mathbf{D}^{-1}\mathbf{C} + \mathbf{K}\right] + \ldots \\ \qquad \mathbf{Q}\mathbf{D}^{-1}\left(-\dot{\mathbf{D}}\mathbf{D}^{-1}\mathbf{M} + \mathbf{C}\right) + \mathbf{R}\mathbf{D}^{-1}\mathbf{M} \\ \mathbf{\Lambda}_1 = \mathbf{P}\mathbf{D}^{-1}\left[\left(2\dot{\mathbf{D}}\mathbf{D}^{-1}\dot{\mathbf{D}}\mathbf{D}^{-1} - \ddot{\mathbf{D}}\mathbf{D}^{-1}\right)\mathbf{C} - 2\dot{\mathbf{D}}\mathbf{D}^{-1}\mathbf{K}\right] + \ldots \\ \qquad \mathbf{Q}\mathbf{D}^{-1}\left(-\dot{\mathbf{D}}\mathbf{D}^{-1}\mathbf{C} + \mathbf{K}\right) + \mathbf{R}\mathbf{D}^{-1}\mathbf{C} \\ \mathbf{\Lambda}_0 = \mathbf{P}\mathbf{D}^{-1}\left(2\dot{\mathbf{D}}\mathbf{D}^{-1}\dot{\mathbf{D}}\mathbf{D}^{-1} - \ddot{\mathbf{D}}\mathbf{D}^{-1}\right)\mathbf{K} - \ldots \\ \qquad \mathbf{Q}\mathbf{D}^{-1}\dot{\mathbf{D}}\mathbf{D}^{-1}\mathbf{K} + \mathbf{R}\mathbf{D}^{-1}\mathbf{K} \end{cases} \tag{37}$$

and

$$\begin{aligned} \mathbf{h}\left(\mathbf{x}, \dot{\mathbf{x}}, \ddot{\mathbf{x}}, \mathbf{x}^{(3)}\right) = \mathbf{P}\mathbf{D}^{-1}\ddot{\mathbf{g}}(\mathbf{x}, \dot{\mathbf{x}}) + \left(-2\mathbf{P}\mathbf{D}^{-1}\dot{\mathbf{D}}\mathbf{D}^{-1} + \mathbf{Q}\mathbf{D}^{-1}\right)\dot{\mathbf{g}}(\mathbf{x}, \dot{\mathbf{x}}) + \ldots \\ \left[\mathbf{P}\mathbf{D}^{-1}\left(2\dot{\mathbf{D}}\mathbf{D}^{-1}\dot{\mathbf{D}}\mathbf{D}^{-1} - \ddot{\mathbf{D}}\mathbf{D}^{-1}\right) - \mathbf{Q}\mathbf{D}^{-1}\dot{\mathbf{D}}\mathbf{D}^{-1} + \mathbf{R}\mathbf{D}^{-1}\right]\mathbf{g}(\mathbf{x}, \dot{\mathbf{x}}) + \mathbf{u}\left(\mathbf{x}, \dot{\mathbf{x}}, \ddot{\mathbf{x}}, \mathbf{x}^{(3)}\right) \end{aligned} \tag{38}$$

The resulting BVPs of Eqs. (27) and (28) require knowledge of the initial conditions $\left(\mathbf{x}_i, \dot{\mathbf{x}}_i, \ddot{\mathbf{x}}_i, \mathbf{x}_i^{(3)}\right)$ at time t_i and the final conditions $\left(\mathbf{x}_f, \dot{\mathbf{x}}_f, \ddot{\mathbf{x}}_f, \mathbf{x}_f^{(3)}\right)$ at time t_f. The initial conditions $\mathbf{x}_i$ and $\dot{\mathbf{x}}_i$ are typically assumed to be deterministic and fixed, whereas $\ddot{\mathbf{x}}_i$ and $\mathbf{x}_i^{(3)}$ are expressed considering Eq. (33) as

$$\ddot{\mathbf{x}}_i = \mathbf{M}^{-1}\left(\mathbf{f}(t_i) - \mathbf{C}\dot{\mathbf{x}}_i - \mathbf{K}\mathbf{x}_i - \mathbf{g}(\mathbf{x}_i, \dot{\mathbf{x}}_i)\right) \tag{39}$$

and

$$\mathbf{x}_i^{(3)} = \mathbf{M}^{-1}\left(\dot{\mathbf{f}}(t_i) - \mathbf{C}\ddot{\mathbf{x}}_i - \mathbf{K}\dot{\mathbf{x}}_i - \dot{\mathbf{g}}(\mathbf{x}_i, \dot{\mathbf{x}}_i)\right) \tag{40}$$

respectively. Taking into account Eqs. (39) and (40) it is readily seen that $\ddot{\mathbf{x}}_i$ and $\mathbf{x}_i^{(3)}$ represent (correlated) random vectors, whose joint PDF $p\left(\ddot{\mathbf{x}}_i, \mathbf{x}_i^{(3)}\right)$, can be determined via the following steps:

i. Apply the WPI technique (e.g., [14]) to Eq. (14) to evaluate the joint PDF of $\boldsymbol{\xi}_s$ and $\dot{\boldsymbol{\xi}}_s$.
ii. $\boldsymbol{\xi}_s$ and $\dot{\boldsymbol{\xi}}_s$ are related to $\mathbf{f}$ and $\dot{\mathbf{f}}$ via Eq. (32), and its differentiated version

$$\dot{\mathbf{f}}(t) = \mathbf{D}(t)\dot{\boldsymbol{\xi}}_s(t) + \dot{\mathbf{D}}(t)\boldsymbol{\xi}_s(t) \tag{41}$$

Thus, the joint PDF $p\left(\ddot{\mathbf{x}}_i, \mathbf{x}_i^{(3)}\right)$ can be readily determined considering Eqs. (39) and (40) and Eqs. (32) and (41), and applying standard PDF transformations between random vectors (e.g., [49]).

Further, taking into account that the initial conditions $\mathbf{x}_i$ and $\dot{\mathbf{x}}_i$ are deterministic and fixed, the response transition PDF is expressed as [39]

$$p\left(\mathbf{x}_f, \dot{\mathbf{x}}_f, \ddot{\mathbf{x}}_f, \mathbf{x}_f^{(3)}, t_f \mid \mathbf{x}_i, \dot{\mathbf{x}}_i, t_i\right) = \int_{-\infty}^{\infty} p\left(\mathbf{x}_f, \dot{\mathbf{x}}_f, \ddot{\mathbf{x}}_f, \mathbf{x}_f^{(3)}, t_f \mid \mathbf{x}_i, \dot{\mathbf{x}}_i, \ddot{\mathbf{x}}_i, \mathbf{x}_i^{(3)}, t_i\right) p\left(\ddot{\mathbf{x}}_i, \mathbf{x}_i^{(3)}\right) \mathrm{d}\ddot{\mathbf{x}}_i \mathrm{d}\mathbf{x}_i^{(3)} \tag{42}$$

The expression in Eq. (42) can be construed as the mean of $p\left(\mathbf{x}_f, \dot{\mathbf{x}}_f, \ddot{\mathbf{x}}_f, \mathbf{x}_f^{(3)}, t_f \mid \mathbf{x}_i, \dot{\mathbf{x}}_i, \ddot{\mathbf{x}}_i, \mathbf{x}_i^{(3)}, t_i\right)$ over all possible initial conditions $\ddot{\mathbf{x}}_i$ and $\mathbf{x}_i^{(3)}$. Overall, to account for stochastic excitation modeling of the form of Eqs. (31) and (32) within the herein developed WPI technique of Section 3.1, $p\left(\mathbf{x}_f, \dot{\mathbf{x}}_f, \ddot{\mathbf{x}}_f, \mathbf{x}_f^{(3)}, t_f \mid \mathbf{x}_i, \dot{\mathbf{x}}_i, \ddot{\mathbf{x}}_i, \mathbf{x}_i^{(3)}, t_i\right)$ is computed for every pair $\left(\ddot{\mathbf{x}}_i, \mathbf{x}_i^{(3)}\right)$ followed by the integration of Eq. (42). This yields one point of the response transition PDF $p\left(\mathbf{x}_f, \dot{\mathbf{x}}_f, \ddot{\mathbf{x}}_f, \mathbf{x}_f^{(3)}, t_f \mid \mathbf{x}_i, \dot{\mathbf{x}}_i, t_i\right)$.

In passing, it is noted that analogous modifications have been devised in alternative stochastic dynamics techniques such as the time-domain formulation of statistical linearization, where the introduction of a “switch” allows the filter equation output to reach stationarity before serving as an input to the original governing equation [6].

3.2.2. Computational aspects

As already discussed in Section 3.1.2, an implementation based on a brute-force discretization of the PDF domain yields N_s^{4m} BVPs to be solved. Further, considering a discretization of the domain of the initial conditions $\ddot{\mathbf{x}}_i$ and $\mathbf{x}_i^{(3)}$ into M points in each dimension, determining one point of $p\left(\mathbf{x}_f, \dot{\mathbf{x}}_f, \ddot{\mathbf{x}}_f, \mathbf{x}_f^{(3)}, t_f \mid \mathbf{x}_i, \dot{\mathbf{x}}_i, t_i\right)$ requires solving M^2 BVPs of Eqs. (27) and (28). Hence, to evaluate the response PDF, $p\left(\mathbf{x}_f, \dot{\mathbf{x}}_f, \ddot{\mathbf{x}}_f, \mathbf{x}_f^{(3)}, t_f \mid \mathbf{x}_i, \dot{\mathbf{x}}_i, t_i\right)$, the number of BVPs to be solved becomes $M^2 N_s^{4m}$. Clearly, the increased number of BVPs to be solved renders the use of the WPI technique in conjunction with the computationally efficient PDF representation schemes proposed in Refs. [14,15] an almost mandatory choice.

4. Numerical examples

In this section, the versatility and reliability of the developed technique are demonstrated by considering various diverse numerical examples. In the first example the technique developed in Section 3.1 is applied to a 2-DOF linear structure under non-white excitation, while to demonstrate the approach delineated in Section 3.2 the second example refers to an SDOF nonlinear oscillator subject to time-modulated non-white excitation. Further, the third example relates to a marine structure subject to flow-induced forces. This example serves to demonstrate that even in cases where the excitation power spectrum (e.g., JONSWAP [50,51]) cannot be analytically expressed in the time domain in the form of Eq. (14), a linear filter approximation [18] provides satisfactory accuracy; and thus, the herein developed WPI technique can be applied in a straightforward manner. Finally, the last example pertains to a cantilever beam with the Young's modulus modeled as a non-white and non-Gaussian stochastic field. In all of the examples, comparisons with corresponding MCS data (50,000 realizations) demonstrate the accuracy of the developed WPI technique. To this aim, a standard fourth-order Runge-Kutta numerical integration scheme is employed for solving the governing equations of motion within the MCS context.

4.1. MDOF system subject to non-white excitation process

To demonstrate the WPI technique developed in Section 3.1, the joint response PDF of an MDOF system exposed to non-white stochastic excitation is determined in this section. Specifically, consider a 2-DOF system, whose equation of motion is given by Eq. (13) with $\mathbf{g}(\mathbf{x}, \dot{\mathbf{x}}) = \mathbf{0}$ and

$$\mathbf{M} = \begin{bmatrix} m_0 & 0 \\ m_0 & m_0 \end{bmatrix} \tag{43}$$

$$\mathbf{C} = \begin{bmatrix} c_0 & -c_0 \\ 0 & c_0 \end{bmatrix} \tag{44}$$

$$\mathbf{K} = \begin{bmatrix} k_0 & -k_0 \\ 0 & k_0 \end{bmatrix} \tag{45}$$

Further, the filter coefficients of Eq. (14) are given by

$$\mathbf{P} = \begin{bmatrix} p & 0 \\ 0 & p \end{bmatrix} \tag{46}$$

$$\mathbf{Q} = \begin{bmatrix} q & 0 \\ 0 & q \end{bmatrix} \tag{47}$$

and

$$\mathbf{R} = \begin{bmatrix} r & 0 \\ 0 & r \end{bmatrix} \tag{48}$$

The parameters used in the numerical example are ($m_0, k_0, p, r = 1$; $q, c_0 = 0.1$; and $S_0 = 0.0637$). Indicatively, the joint PDF of x_1 and x_2 is plotted at time instants $t = 1.0$ s and $t = 2.0$ s in Figs. 1 and 2, respectively, whereas the corresponding marginal PDFs are plotted in Fig. 3. Pertinent MCS data are included in the figures for comparison purposes as well. Following [14], the joint response transition PDF is approximated by a second-order polynomial. In this regard, for a given time instant t_f, solving only 37 BVPs of the form of Eqs. (27) and (28), the polynomial expansion coefficients are obtained and the complete PDF is readily available at any point $\left(\mathbf{x}_f, \dot{\mathbf{x}}_f, \ddot{\mathbf{x}}_f, \mathbf{x}_f^{(3)}\right)$. It is readily seen that the results obtained via the proposed technique are in very good agreement with the MCS data, demonstrating the capability of the developed WPI technique to capture the salient features of the system joint response PDF.

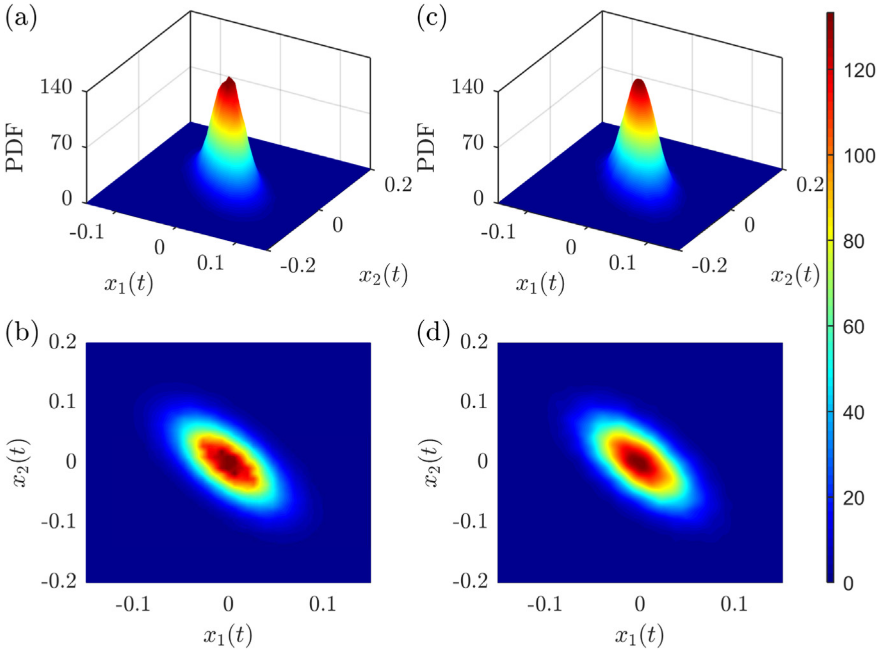

Fig. 1. Joint PDF of $x_1(t)$ and $x_2(t)$ at time $t = 1.0$s, as obtained via the WPI technique (a–b); comparisons with MCS data - 50,000 realizations (c–d).

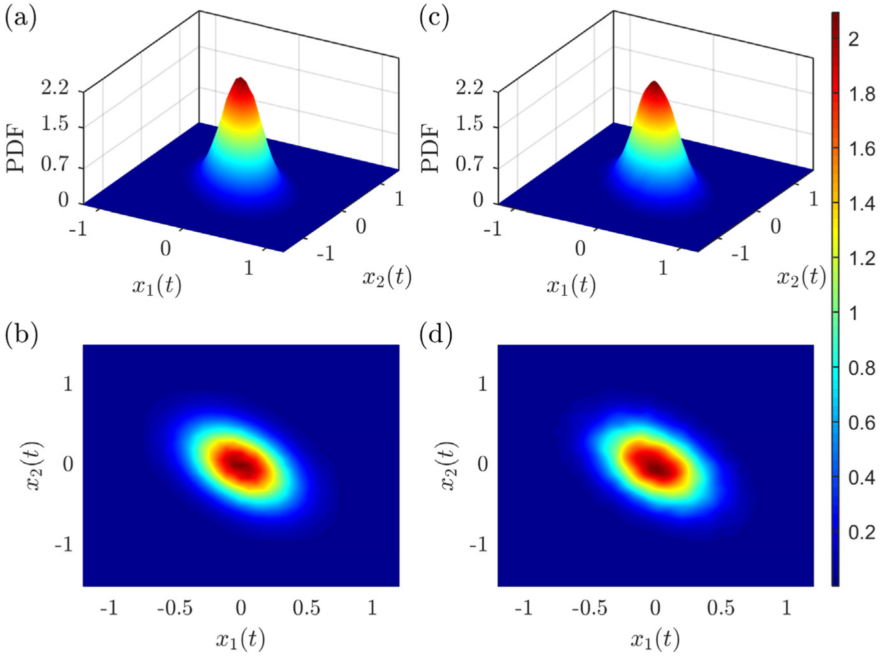

Fig. 2. Joint PDF of $x_1(t)$ and $x_2(t)$ at time $t = 2.0$s, as obtained via the WPI technique (a–b); comparisons with MCS data - 50,000 realizations (c–d).

4.2. SDOF system subject to time-modulated non-white excitation process

To demonstrate the modification of the technique (as delineated in Section 3.2) to allow the filter equation output to reach stationarity, a nonlinear SDOF oscillator is considered in this example. The motion of the oscillator is governed by Eq. (33) with ($\mathbf{M} = m_0 = 1$; $\mathbf{C} = c_0 = 0.1$; $\mathbf{K} = k_0 = 2$; $\mathbf{g}(\mathbf{x}, \dot{\mathbf{x}}) = \epsilon k_0 x^3$; and $\epsilon = 1$), where ϵ represents the nonlinearity magnitude. The excitation $f(t)$ is modeled according to Eqs. (31) and (32) with a power spectrum given by

$$S_f(\omega, t) = d^2(t) S_{\xi_s}(\omega) \tag{49}$$

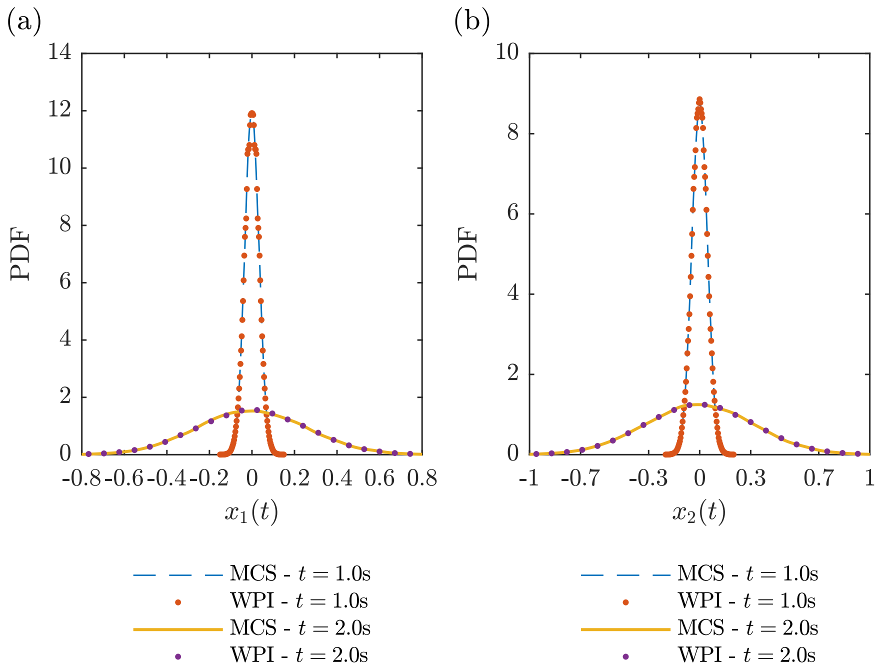

Fig. 3. Marginal PDF of $x_1(t)$ (a) and $x_2(t)$ (b) at time instants $t = 1.0$ s and $t = 2.0$ s, as obtained via the WPI technique; comparisons with MCS data (50,000 realizations).

where

$$S_{\xi_s}(\omega) = \frac{S_0}{\omega^2 q^2 + r^2} \tag{50}$$

and

$$d(t) = \gamma + \lambda(e^{-\alpha t} - e^{-\beta t}) \tag{51}$$

The parameters in Eq. (51) are selected to be ($\alpha = 1$; $\beta = 2$; $\gamma = 10^{-4}$; and $\lambda = 4$). Note that $S_{\xi_s}(\omega)$ corresponds to the stationary output of the time-domain filter equation

$$q\dot{\xi} + r\xi = w(t) \tag{52}$$

where $q = 1$; $r = 1$; and $w(t)$ is a zero-mean white noise process with intensity $S_0 = 1$. Next, applying Eqs. (34) and (35), $\xi_s(t)$ and $\dot{\xi}_s(t)$ are expressed in terms of $f(t)$ and substituted into Eq. (52), yielding

$$\frac{1}{d}\left[r\left(m_0\ddot{x} + c_0\dot{x} + k_0x + \epsilon k_0x^3\right) + q\left(m_0x^{(3)} + c_0\ddot{x} + k_0\dot{x} + 3\epsilon k_0x^2\dot{x} - \dot{d}/d\left(m_0\ddot{x} + c_0\dot{x} + k_0x + \epsilon k_0x^3\right)\right)\right] = w(t) \tag{53}$$

Note that the associated Lagrangian takes the form

$$L\left[x, \dot{x}, \ddot{x}, x^{(3)}\right] = \frac{1}{4\pi S_0}\frac{1}{d^2}\left[r(m_0\ddot{x} + c_0\dot{x} + \dots\right.$$
$$\left. k_0x + \epsilon k_0x^3) + q\left(m_0x^{(3)} + c_0\ddot{x} + k_0\dot{x} + 3\epsilon k_0x^2\dot{x} - \dot{d}/d\left(m_0\ddot{x} + c_0\dot{x} + k_0x + \epsilon k_0x^3\right)\right)\right]^2 \tag{54}$$

whereas the corresponding E-L Eq. (27) becomes

$$\frac{\partial L}{\partial x_c} - \frac{\partial}{\partial t}\frac{\partial L}{\partial \dot{x}_c} + \frac{\partial^2}{\partial t^2}\frac{\partial L}{\partial \ddot{x}_c} - \frac{\partial^3}{\partial t^3}\frac{\partial L}{\partial x_c^{(3)}} = 0 \tag{55}$$

together with the initial conditions for $t_i = 0$, $x_c(t_i) = x_i = 0$, $\dot{x}_c(t_i) = \dot{x}_i = 0$ and $\ddot{x}_c(t_i) = \ddot{x}_i = \frac{1}{m_0}d(t_i)\xi_s(t_i)$. As noted in Section 3.2.1, $\ddot{x}_i$ is a random variable. In the following, first, the WPI technique is utilized [14] in conjunction with the filter Eq. (52) for determining the stationary PDF $p_{\xi_s}\left(\xi_s(t_i)\right)$, and second, the PDF $p_{\ddot{x}_i}(\ddot{x}_i)$ is computed via the relationship [49]

$$p_{\ddot{x}_i}(\ddot{x}_i) = \frac{m_0}{d(t_i)}\left[p_{\xi_s}\left(\frac{m_0}{d(t_i)}\ddot{x}_i\right)\right] \tag{56}$$

Further, a domain of initial conditions, $\ddot{x}_i$, is considered and discretized into $M = 30$ points. In addition, an effective domain of final conditions, x_f, $\dot{x}_f$ and $\ddot{x}_f$, is also considered and discretized into $N_s = 101$ points in each dimension (see also Section 3.2.2).

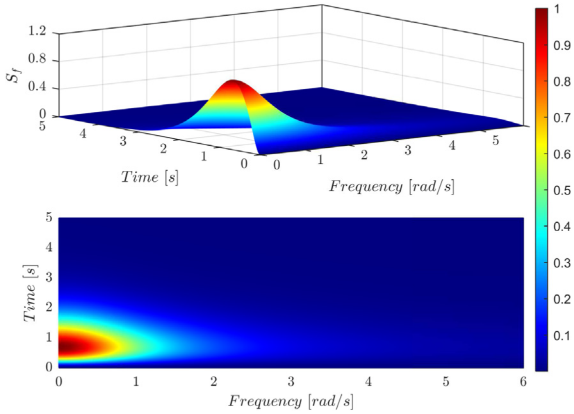

Fig. 4. Excitation evolutionary Power Spectrum, given by Eq. (49) with parameter values ($q = 1$; $r = 1$; $S_0 = 1$; $\alpha = 1$; $\beta = 2$; $\gamma = 10^{-4}$; and $\lambda = 4$).

Hence, for each set of final conditions $(x_f, \dot{x}_f, \ddot{x}_f)$, $M^2 = 900$ BVPs of the form of Eq. (55) are solved. Each BVP solution yields a most probable path, $x_c(t)$, which is substituted into Eq. (29) yielding

$$p(x_f, \dot{x}_f, \ddot{x}_f, t_f \mid x_i, \dot{x}_i, \ddot{x}_i, t_i) = \exp\left(-\int_{t_i}^{t_f} L\left[x_c, \dot{x}_c, \ddot{x}_c, x_c^{(3)}\right] \mathrm{d}t \right) \tag{57}$$

Subsequently, a point of the PDF $p(x_f, \dot{x}_f, \ddot{x}_f, t_f \mid x_i, \dot{x}_i, t_i)$ is determined by employing Eq. (42), i.e.,

$$p(x_f, \dot{x}_f, \ddot{x}_f, t_f \mid x_i, \dot{x}_i, t_i) = \int_{-\infty}^{\infty} p\left(x_f, \dot{x}_f, \ddot{x}_f, t_f \mid x_i, \dot{x}_i, \ddot{x}_i, t_i\right) p_{\ddot{x}_i}(\ddot{x}_i)\mathrm{d}\ddot{x}_i \tag{58}$$

Next, to assess the performance of the developed approximate technique, comparisons are made between the nonstationary response displacement and velocity PDFs determined by the WPI technique and by MCS data (50, 000 realizations). For the MCS, the spectral representation technique [52,53] is employed to generate realizations of $f(t)$ compatible with the evolutionary power spectrum of Eq. (49), which is also plotted in Fig. 4.

Figs. 5 and 6 show the joint PDF of $x(t)$ and $\dot{x}(t)$ at $t = 0.5$s and $t = 1.0$s, respectively. Moreover, Fig. 7 shows the marginal PDFs of $x(t)$ and $\dot{x}(t)$ at $t = 0.5$ s and $t = 1.0$ s, as obtained by the herein developed WPI technique and by MCS data (50, 000 realizations). Overall, the results obtained via the WPI technique agree very well with the MCS data, however, it is noted that the computational cost becomes prohibitive for relatively high dimensional MDOF systems. In this regard, an efficient numerical treatment for determining the joint response PDF, such as the one proposed by Kougioumtzoglou et al. [14], becomes necessary.

4.3. Structural system exposed to flow-induced forces

Next, an example pertaining to a structure exposed to flow-induced forces is presented. This kind of problem is encountered frequently in marine engineering applications, as structures composed by slender elements are excited by flow-induced forces which are described commonly via the Morison equation [54]. The salient features of the Morison equation are the use of an inertial force proportional to the mass of the system and the computation of a drag-type nonlinearity accounting for the relative velocity between the structure and the water particles. Indicative examples of such structures include the tension leg platforms [55], the jacket structures [56] and the spar structures [57].

In addition to the nonlinearity related to the flow-induced forces, this class of problems is characterized by random excitations with non-white power spectra dependent on the free surface power spectrum of the underlying sea state. In this regard, note that classical models of sea wave spectra have been proposed, for instance, by Pierson and Moskowitz [50] and by Hasselmann et al. [51] (the celebrated JONSWAP spectrum). In these models, the spectrum of the free surface displacement is described by the equation, in nondimensional form,

$$S(\overline{\omega}) = \frac{S(\omega)}{S(\omega_p)} = \frac{\exp(1.25)}{\overline{\omega}^5} \exp\left(-\frac{1.25}{\overline{\omega}^4}\right) \gamma^{\mu-1} \tag{59}$$

where

$$\overline{\omega} = \frac{\omega}{\omega_p} \tag{60}$$

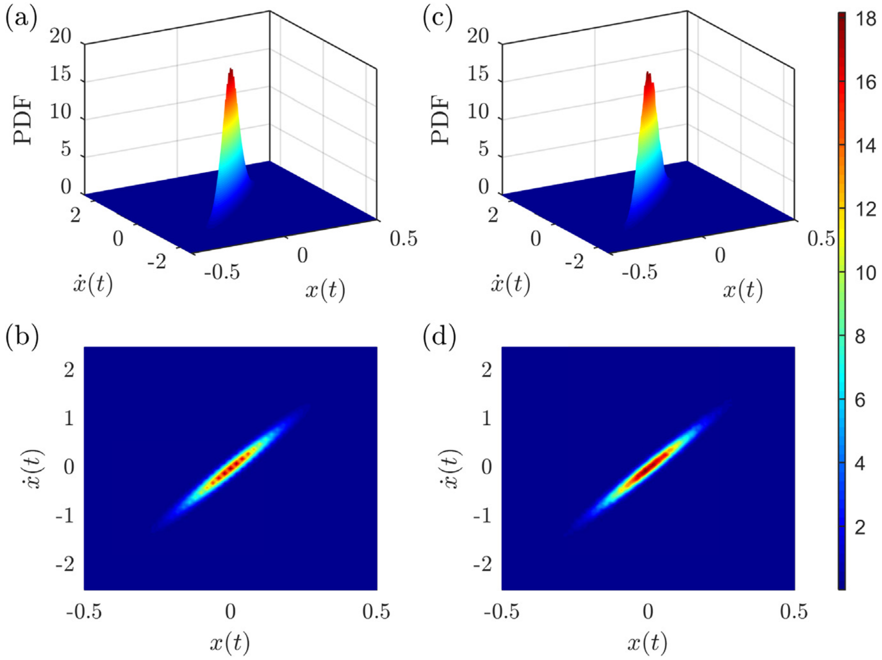

Fig. 5. Joint PDF of $x(t)$ and $\dot{x}(t)$ at time $t = 0.5$ s, as obtained via the WPI technique (a–b); comparisons with MCS data - 50,000 realizations (c–d).

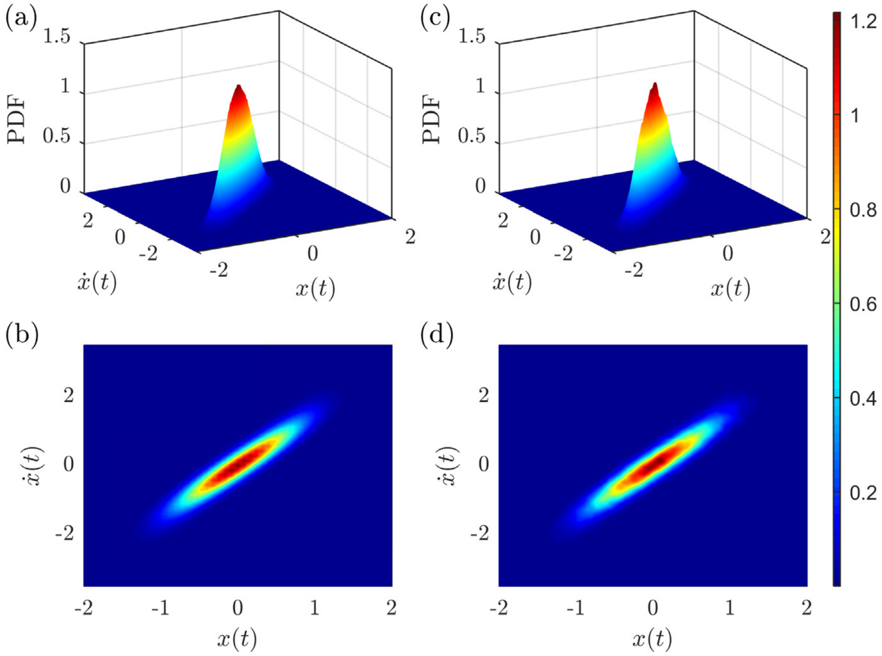

Fig. 6. Joint PDF of $x(t)$ and $\dot{x}(t)$ at time $t = 1.0$ s, as obtained via the WPI technique (a–b); comparisons with MCS data - 50, 000 realizations (c–d).

and

$$\gamma = \exp\left[-\frac{(1-\overline{\omega})^2}{2\lambda^2}\right] \tag{61}$$

with γ denoting the peak enhancement factor; λ the sharpness magnification factor; and ω_p the peak frequency of the spectrum.

In the current example the linear oscillator

$$m_0\ddot{x} + c_0\dot{x} + k_0x = h(t) \tag{62}$$

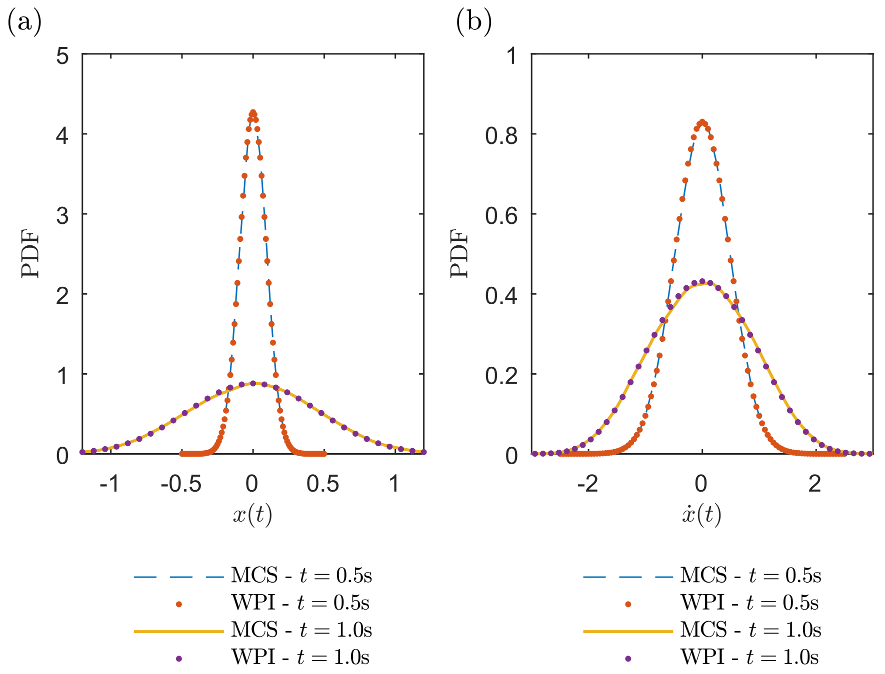

Fig. 7. Marginal PDF of $x(t)$ (a) and $\dot{x}(t)$ (b) at time instants $t = 0.5$ s and $t = 1.0$ s, as obtained via the WPI technique; comparisons with MCS data (50,000 realizations).

is considered, where m_0 is the mass of the system; c_0 its structural damping; k_0 the structural stiffness; x the absolute displacement of the structure; and $h(t)$ the system excitation. $h(t)$ is calculated as [58]

$$h(t) = \rho A\ddot{v} + C_l \rho A(\ddot{v} - \ddot{x}) + \frac{1}{2}C_D \rho D|\dot{v} - \dot{x}|(\dot{v} - \dot{x}) \tag{63}$$

with ρ being the water density; A the cross-sectional area of the structure; D its diameter; C_l and C_D the mass and drag coefficients, respectively; and $\dot{v}$ the water particle velocity. Utilizing the relative coordinates $y = x - v$, the equation of motion is recast as

$$\ddot{y} + 2\omega_N \xi_N \dot{y} + \omega_N^2 y + \frac{1}{2}\frac{C_D \rho D}{M_0}|V + \dot{y}|(V + \dot{y}) = f(t) \tag{64}$$

In Eq. (64) Vdenotes the water current (mean component of the water particle velocity); $M_0 = m_0 + C_l \rho A$; and $f(t)$ denotes the system excitation which is compatible with the power spectrum [58]

$$S_f(\omega) = \left[\omega_N^4 + \left(2\xi_N - 2 + 2C_M \frac{\rho A}{M_0}\right)\omega_N^2 \omega^2 + \left(1 - C_M \frac{\rho A}{M_0}\right)^2 \omega^4\right] S(\omega) \tag{65}$$

with

$$C_M = 1 + C_l \tag{66}$$

$$\omega_N = \omega_0 \sqrt{\frac{m_0}{M_0}} \tag{67}$$

and

$$\xi_N = c_0 \sqrt{\frac{m_0}{M_0}} \tag{68}$$

Next, the proposed WPI technique is implemented by approximating the excitation power spectrum (Eq. (65)) via the second-order linear filter

$$p\ddot{f}(t) + q\dot{f}(t) + rf(t) = w(t) \tag{69}$$

Hence, the system dynamics is described by the system of equations

$$\begin{cases} \ddot{y} + 2\omega_N \xi_N \dot{y} + \omega_N^2 y + \frac{1}{2}\frac{C_D \rho D}{M_0}|V + \dot{y}|(V + \dot{y}) = f(t) \\ p\ddot{f}(t) + q\dot{f}(t) + rf(t) = w(t) \end{cases} \tag{70}$$

Table 1
System parameters pertaining to Eq. (70).

ξ_N	$\rho D/M_0$	V[m/s]	C_D	ω_N	C_M	$A[m^2]$	$D[m]$
0.02	1.136	0	1	1.2566	1.25	0.073	0.30

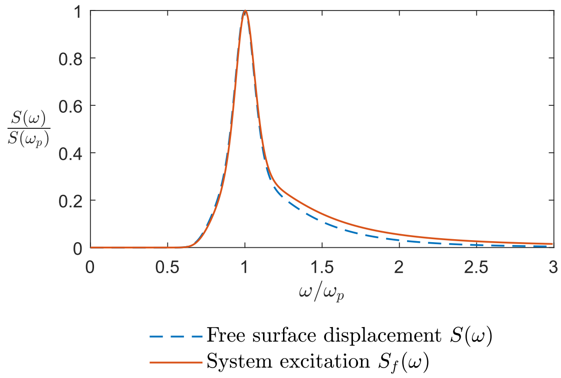

Fig. 8. Comparison between the normalized power spectra of the free surface displacement and of the system excitation Eq. (64).

Note that the use of a second-order linear filter is not restrictive. Indeed, higher-order filters can be considered as well to enhance the accuracy of the filter approximation to a desired level. In this regard, relevant studies have been pursued by Spanos [18] and more recently by Chai et al. [19] regarding the identification of the filter parameters and the impact on the structural response determination.

The numerical example is conducted by considering the input parameters shown in Table 1 and a free surface displacement spectrum $S(\omega)$ compatible with a mean JONSWAP spectrum having significant wave height $H_S = 1$ m. Such a system is exposed to a force with the power spectrum shown in Fig. 8. More specifically, Fig. 8 shows that the spectrum of the excitation is bell-shaped. Further, a comparison with the corresponding free surface displacement spectrum $S(\omega)$ shows that they have a similar low frequency pattern and the same peak frequencies, however, the free surface spectrum decays more rapidly at higher frequencies.

The proposed WPI technique is implemented by approximating first the system excitation via the second-order filter with parameters (p, q, r) (see Eq. (70)). For this purpose, a least squares numerical optimization scheme is utilized for estimating the parameters that minimize the mean square error between the excitation spectrum and the filter approximation in the frequency domain. This procedure produces the optimal filter parameters shown in Table 2, corresponding to the power spectrum shown in Fig. 9 with dashed line.

To assess the reliability of the technique, MCS studies (50,000 realizations) are performed and corresponding data are compared with the approximate PDF determined by the WPI technique. For the WPI solution, the domain of final points $\left(y_f, \dot{y}_f, \ddot{y}_f, y_f^{(3)}\right)$ is discretized into 51 points in each dimension and the marginal PDFs are obtained by numerical integration. The initial conditions are considered deterministic and equal to $\left(y_i = 0; \dot{y}_i = 0; \ddot{y}_i = 0; y_i^{(3)} = 0\right)$. Figs. 10 and 11 show the joint PDF of displacement and velocity related to the final time instants $t = 0.5$ s and $t = 1.0$ s, respectively. Fig. 12 shows the marginal displacement and velocity PDFs at time instants $t = 0.5$ s and $t = 1.0$ s, while comparisons with MCS based PDFs demonstrate a high degree of accuracy.

Overall, it is seen that even for arbitrary forms of excitation power spectra, the use of a filter approximation facilitates the implementation of the WPI technique in a straightforward manner.

Table 2
Parameters of the filter (Eq. (69)) and (constant) value of the spectrum (S_0) associated with the white noise input of the filter.

p	q	r	S_0
18.98	4.59	31.39	17.18

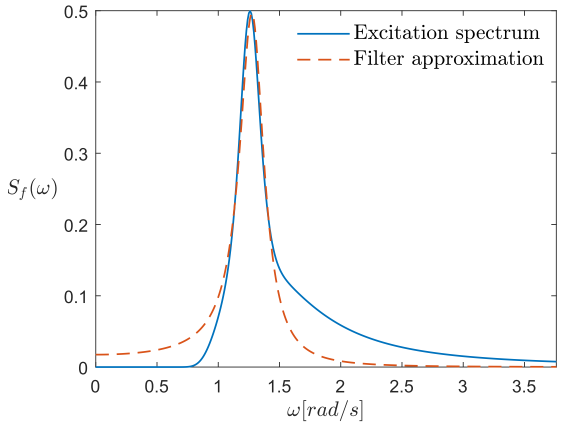

Fig. 9. Comparison between the excitation spectrum (solid line) and its filter approximation (dashed line).

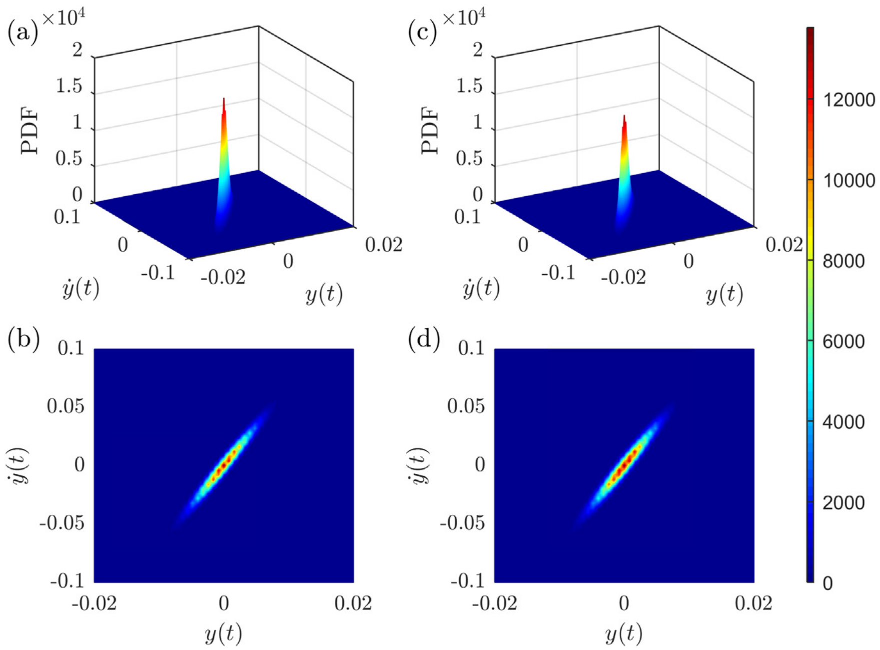

Fig. 10. Joint PDF of $y(t)$ and $\dot{y}(t)$ at time $t = 0.5$ s, as obtained via the WPI technique (a–b); comparisons with MCS data - 50,000 realizations (c–d).

4.4. Beam bending problem with stochastic Young's modulus

Consider next a statically determinate Euler-Bernoulli beam satisfying the differential equation

$$\frac{\mathrm{d}^2}{\mathrm{d}z^2}\left[E(z)I\ddot{q}(z)\right] = l(z) \tag{71}$$

where $E(z)$ is the Young's modulus; I is the constant cross-sectional moment of inertia; $q(z)$ is the deflection of the beam; and $l(z)$ denotes a deterministic distributed force. Clearly, in this static problem the dot above a variable denotes differentiation with respect to the space variable z. Further, as pointed out by Shinozuka [59] and Kougioumtzoglou [16], the fact that the structure is statically determinate allows for integrating twice Eq. (71) under the boundary conditions $-E(z)I\ddot{q}(z) = M_0$ at $z = 0$ and $-E(z)I\ddot{q}(z) = M_L$ at $z = L$ yielding

$$-E(z)I\ddot{q}(z) = M(z) \tag{72}$$

where L is the length of the beam, and $M(z)$ is the bending moment of the beam. Alternatively, Eq. (72) can be cast in the form

$$-\frac{M(z)}{I\ddot{q}(z)} = E(z) \tag{73}$$

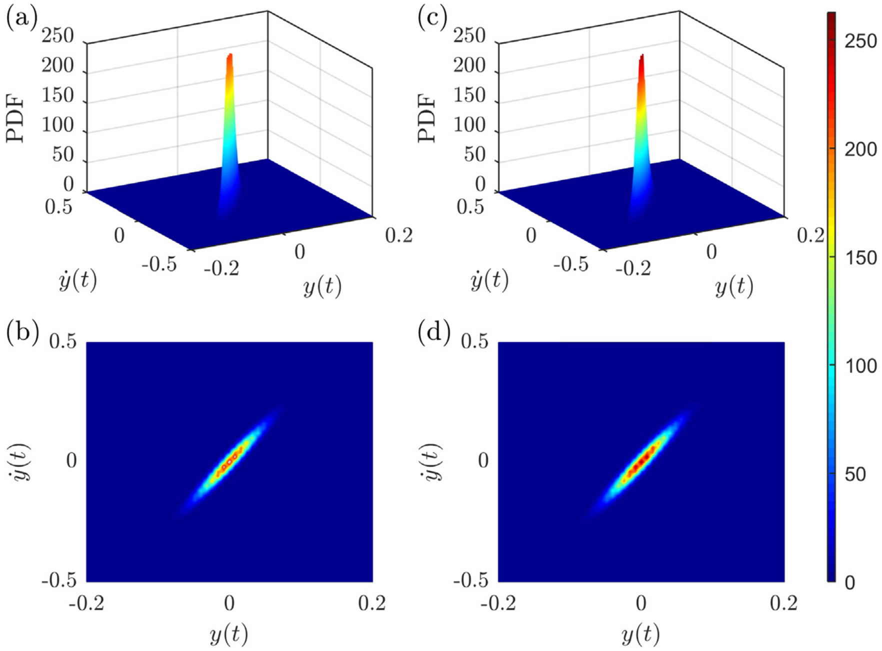

Fig. 11. Joint PDF of $y(t)$ and $\dot{y}(t)$ at time $t = 1.0$ s, as obtained via the WPI technique (a–b); comparisons with MCS data - 50,000 realizations (c–d).

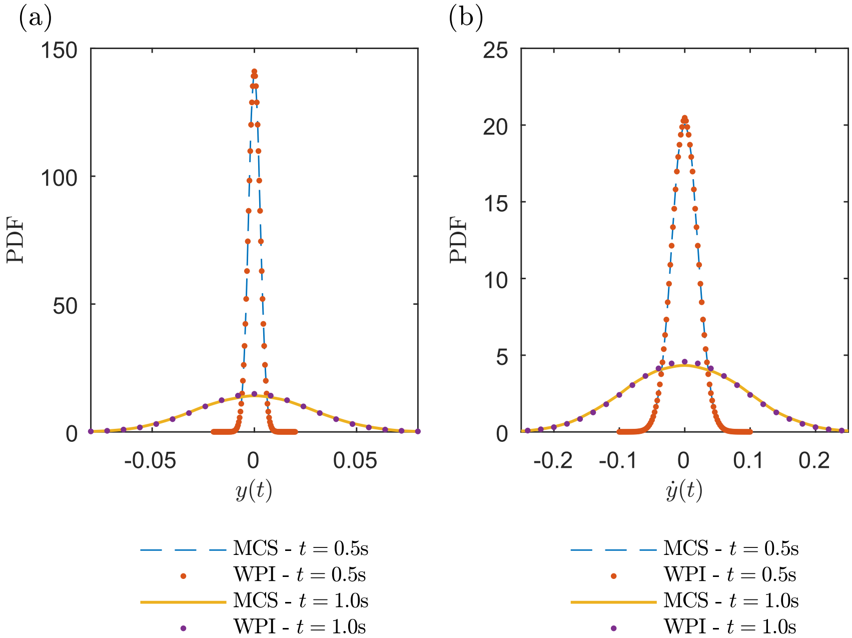

Fig. 12. Marginal PDF of $y(t)$ (a) and $\dot{y}(t)$ (b) at time instants $t = 0.5$ s and $t = 1.0$ s, as obtained via the WPI technique; comparisons with MCS data (50,000 realizations).

In the following, the Young's modulus is modeled as a non-Gaussian, non-white and non-homogeneous stochastic field as

$$\frac{\dot{E}(z)}{E(z)} = w(z) \tag{74}$$

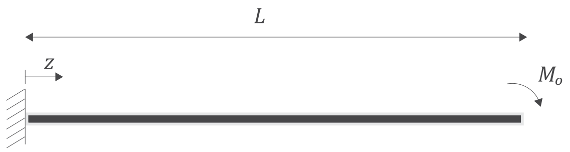

Fig. 13. Cantilever beam subject to a single-point moment.

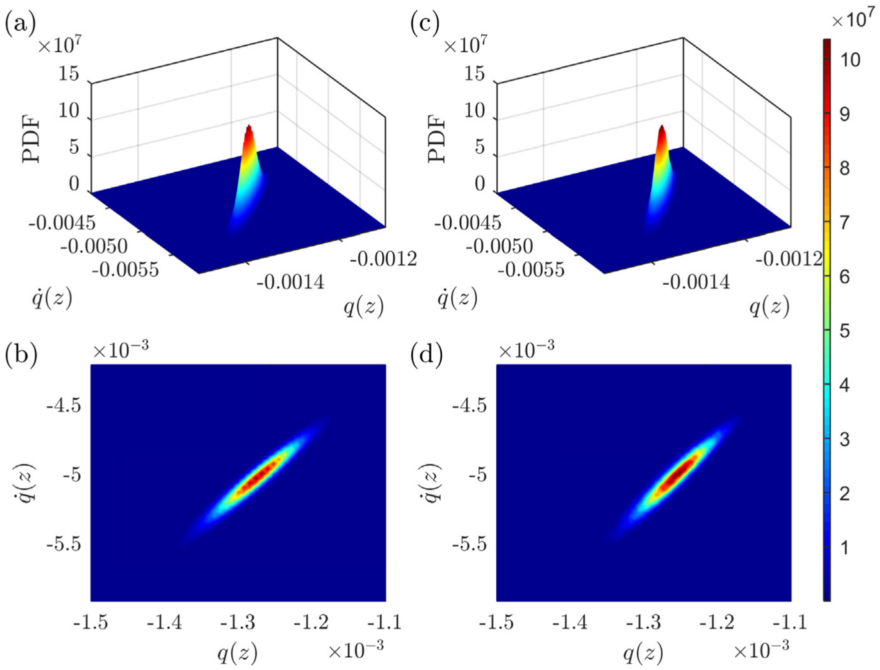

Fig. 14. Joint PDF of $q(z)$ and $\dot{q}(z)$ at position $z = 0.5$, as obtained via the WPI technique (a–b); comparisons with MCS data - 50,000 realizations (c–d).

with $E(0) = E_M$, and $w(z)$ is the white noise process as defined in Eq. (14). It can be readily seen that Eq. (74) represents a standard geometric Brownian motion SDE, whose space-dependent response PDF is log-normal (e.g., [60]).

Further, combining Eqs. (73) and (74) yields an equation in the form of Eq. (16); that is,

$$\frac{\dot{M}(z)}{M(z)} - \frac{q^{(3)}(z)}{\ddot{q}(z)} = w(z) \tag{75}$$

Next, the case of a cantilever beam subject to a single point moment at its free end is considered (Fig. 13). Thus, taking into account that $M(z)$ is constant along the length of the beam, i.e., $M(z) = M_0$, Eq. (75) becomes

$$-\frac{q^{(3)}(z)}{\ddot{q}(z)} = w(z) \tag{76}$$

while the Lagrangian given by Eq. (25) yields

$$L\left[q, \dot{q}, \ddot{q}, q^{(3)}\right] = \frac{(q^{(3)}(z))^2}{4\pi S_0(\ddot{q}(z))^2} \tag{77}$$

The E-L equation becomes

$$\frac{\partial L}{\partial q_c} - \frac{\partial}{\partial z}\frac{\partial L}{\partial \dot{q}_c} + \frac{\partial^2}{\partial z^2}\frac{\partial L}{\partial \ddot{q}_c} - \frac{\partial^3}{\partial z^3}\frac{\partial L}{\partial q_c^{(3)}} = 0 \tag{78}$$

together with the initial conditions for $z_i = 0$, $q_c(z_i) = q_i = 0$, $\dot{q}_c(z_i) = \dot{q}_i = 0$ and $\ddot{q}_c(z_i) = -\frac{M_0}{E_M I}$.

Figs. 14 and 15 show the joint PDF of $q(z)$ and $\dot{q}(z)$ for various points along the length of the beam and for parameter values ($E_M = 10^6; I = 10; M_0 = 10^5; L = 1$; and $S_0 = 0.001$), obtained by the WPI technique and compared with MCS data (50, 000 realizations). Moreover, Figs. 16 and 17 show the marginal PDFs of $q(z)$ and $\dot{q}(z)$, respectively.

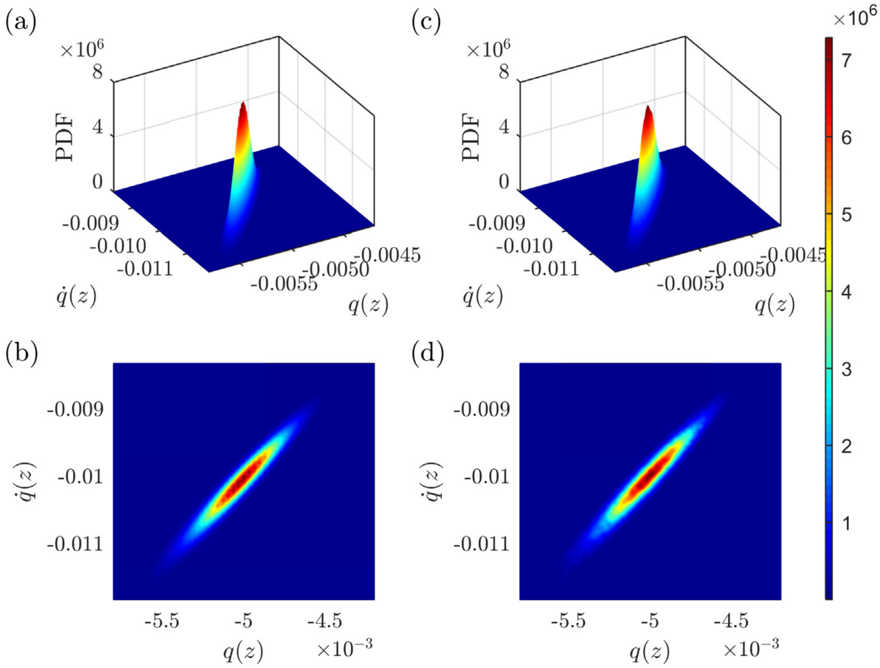

Fig. 15. Joint PDF of $q(z)$ and $\dot{q}(z)$ at position $z = 1.0$, as obtained via the WPI technique (a–b); comparisons with MCS data - 50,000 realizations (c–d).

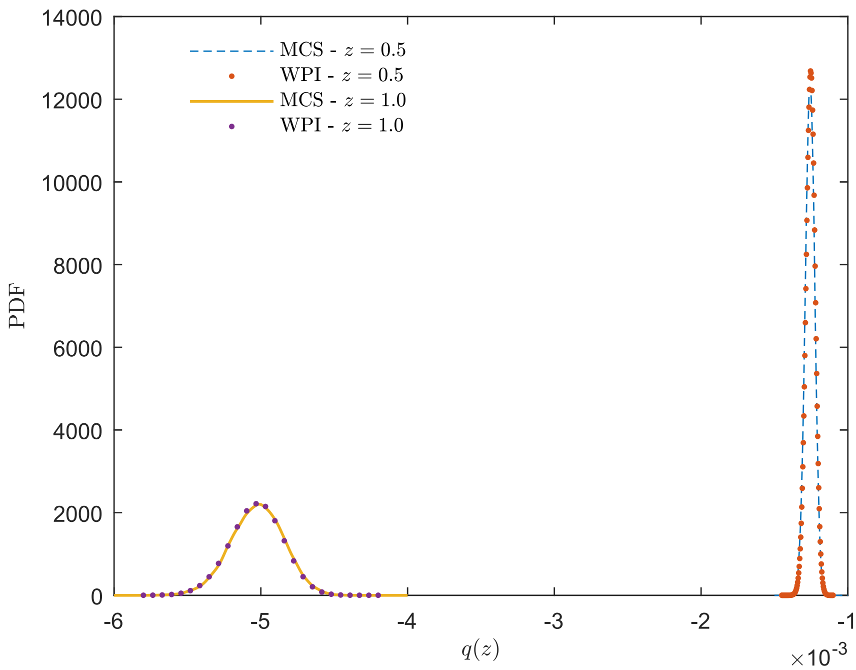

Fig. 16. PDF of $q(z)$ at positions $z = 0.5$ and $z = 1.0$, as obtained via the WPI technique; comparisons with MCS data (50,000 realizations).

Overall, it is seen that the herein developed WPI technique exhibits relatively high accuracy and appears capable of capturing the salient features of the response PDF. Further, a significant advantage relates to the fact that the technique can be used not only for random vibration problems with stochastic excitations, but also for various stochastic mechanics problems (such as the beam bending example) with stochastic material/media properties that can be cast in the form of Eq. (13) and (14). In this regard, it has been demonstrated in this example that physically realistic modeling of material properties as non-Gaussian, non-white, and non-homogeneous stochastic fields can be readily accounted for.

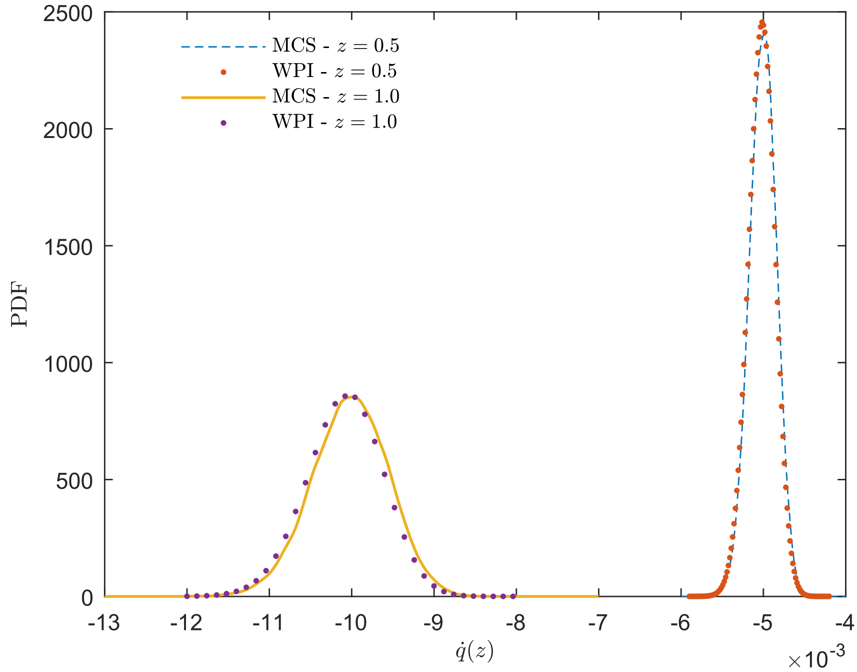

Fig. 17. PDF of $\dot{q}(z)$ at positions $z = 0.5$ and $z = 1.0$, as obtained via the WPI technique; comparisons with MCS data (50,000 realizations).

5. Conclusion

A generalization of the WPI technique has been developed in this paper to account for non-Gaussian, non-white and non-stationary excitation processes. In this regard, the excitation process has been modeled as the output of a filter equation with Gaussian white noise as its input, while the response process vector has been augmented to account for the additional filter equation. It has been shown that even in cases where the excitation power spectrum cannot be cast in a convenient form in the time domain, a filter approximation facilitates the application of the technique. Further, it has been demonstrated that the technique can also address a class of continuous systems [16] with media properties modeled as non-Gaussian and non-homogeneous stochastic fields.

Regarding the computational cost, it has been shown that the technique can be readily coupled with recently developed computationally efficient PDF expansion schemes such as the one by Kougioumtzoglou et al. [14]; see also Psaros et al. [15]. Overall, the developments in this paper have increased significantly the versatility of WPI technique, while comparisons with pertinent MCS data demonstrate a high degree of accuracy.

Acknowledgements

I. A. Kougioumtzoglou gratefully acknowledges the support through his CAREER award by the CMMI Division of the National Science Foundation, USA (Award number: 1748537)

G. Malara acknowledges support by the Marie Curie IRSES project “Large Multi-Purpose Platforms for Exploiting Renewable Energy in Open Seas (PLENOSE)”, funded by the European Union (Grant Agreement Number: PIRSES-GA-2013-612581).

References

[1] P.D. Spanos, B.A. Zeldin, Monte Carlo treatment of random fields: a broad perspective, Appl. Mech. Rev. 51 (3) (1998) 219–237.
[2] R.Y. Rubinstein, D.P. Kroese, Simulation and the Monte Carlo Method, second ed., Wiley, Hoboken, NJ, 2007.
[3] J.B. Roberts, P.D. Spanos, Stochastic averaging: an approximate method of solving random vibration problems, Int. J. Non Lin. Mech. 21 (2) (1986) 111–134.
[4] W.Q. Zhu, Recent developments and applications of the stochastic averaging method in random vibration, Appl. Mech. Rev. 49 (10S) (1996) 72–80.
[5] P.D. Spanos, I.A. Kougioumtzoglou, C. Soize, On the determination of the power spectrum of randomly excited oscillators via stochastic averaging: an alternative perspective, Probabilist. Eng. Mech. 26 (1) (2011) 10–15.
[6] J.B. Roberts, P.D. Spanos, Random Vibration and Statistical Linearization, Dover, New York, 2003.
[7] P.D. Spanos, I.A. Kougioumtzoglou, Harmonic wavelets based statistical linearization for response evolutionary power spectrum determination, Probabilist. Eng. Mech. 27 (1) (2012) 57–68.
[8] V.C. Fragkoulis, I.A. Kougioumtzoglou, A.A. Pantelous, Statistical linearization of nonlinear structural systems with singular matrices, J. Eng. Mech. 142 (9) (2016) 04016063.
[9] Y.-K. Lin, Probabilistic Theory of Structural Dynamics, Krieger Publishing Company, 1976.
[10] M. Chaichian, A. Demichev, Path Integrals in Physics: Stochastic Processes and Quantum Mechanics, Institute of Physics Publishing, Bristol, U.K., 2001.

[11] I.A. Kougioumtzoglou, P.D. Spanos, An analytical Wiener Path Integral technique for non-stationary response determination of nonlinear oscillators, Probabilist. Eng. Mech. 28 (2012) 125–131.
[12] I.A. Kougioumtzoglou, P.D. Spanos, Nonstationary stochastic response determination of nonlinear systems: a Wiener Path Integral formalism, J. Eng. Mech. 140 (9) (2014) 04014064.
[13] A. Di Matteo, I.A. Kougioumtzoglou, A. Pirrotta, P.D. Spanos, M. Di Paola, Stochastic response determination of nonlinear oscillators with fractional derivatives elements via the Wiener Path Integral, Probabilist. Eng. Mech. 38 (2014) 127–135.
[14] I.A. Kougioumtzoglou, A. Di Matteo, P.D. Spanos, A. Pirrotta, M. Di Paola, An efficient Wiener Path Integral technique formulation for stochastic response determination of nonlinear MDOF systems, J. Appl. Mech. 82 (10) (2015) 101005.
[15] A.F. Psaros, I.A. Kougioumtzoglou, I. Petromichelakis, Sparse representations and compressive sampling for enhancing the computational efficiency of the Wiener path integral technique, Mech. Syst. Signal Process. 111 (2018) 87–101.
[16] I.A. Kougioumtzoglou, A wiener path integral solution treatment and effective material properties of a class of one-dimensional stochastic mechanics problems, J. Eng. Mech. 143 (6) (2017) 04017014.
[17] A.T. Meimaris, I.A. Kougioumtzoglou, A.A. Pantelous, A closed form approximation and error quantification for the response transition probability density function of a class of stochastic differential equations, Probabilist. Eng. Mech. (2017), https://doi.org/10.1016/j.probengmech.2017.07.005.
[18] P.D. Spanos, Filter approaches to wave kinematics approximation, Appl. Ocean Res. 8 (1) (1986) 2–7.
[19] W. Chai, A. Naess, B.J. Leira, Filter models for prediction of stochastic ship roll response, Probabilist. Eng. Mech. 41 (2015) 104–114.
[20] T. Soong, M. Grigoriu, Random Vibration of Mechanical and Structural Systems, Prentice Hall, New Jersey, 1993.
[21] I. Gihman, A. Skorohod, Stochastic Differential Equations, Springer–Verlag Berlin Heidelberg, 1972.
[22] C. Gardiner, Stochastic Methods: a Handbook for the Natural and Social Sciences, Springer–Verlag Berlin Heidelberg, 2009.
[23] L. Arnold, Stochastic Differential Equations: Theory and Applications, Wiley, New York, 1974.
[24] M. Grigoriu, Stochastic Calculus: Applications in Science and Engineering, Birkhäuser Basel, 2002.
[25] H. Risken, The Fokker-planck Equation. Methods of Solution and Applications, Springer-Verlag, Berlin, 1996.
[26] F. Langouche, D. Roekaerts, E. Tirapegui, Functional integrals and the Fokker-Planck equation, Il Nuovo Cimento 53 (1) (1979) 135–159 (1971-1996).
[27] A. Naess, V. Moe, Stationary and non-stationary random vibration of oscillators with bilinear hysteresis, Int. J. Non Lin. Mech. 31 (5) (1996) 553–562.
[28] M.F. Wehner, W. Wolfer, Numerical evaluation of path-integral solutions to Fokker-Planck equations, Phys. Rev. 27 (5) (1983) 2663.
[29] A. Naess, J. Johnsen, Response statistics of nonlinear, compliant offshore structures by the path integral solution method, Probabilist. Eng. Mech. 8 (2) (1993) 91–106.
[30] M. Di Paola, R. Santoro, Path integral solution for non-linear system enforced by Poisson white noise, Probabilist. Eng. Mech. 23 (2–3) (2008) 164–169.
[31] P. Alevras, D. Yurchenko, GPU computing for accelerating the numerical Path Integration approach, Comput. Struct. 171 (2016) 46–53.
[32] R.P. Feynman, A.R. Hibbs, D.F. Styer, Quantum Mechanics and Path Integrals, Emended Edition, Dover Books on Physics, 2010.
[33] K. Kanai, Semi-empirical formula for the seismic characteristics of the ground, Bull. Earthq. Res. Inst. 35 (1957) 309–325.
[34] H. Tajimi, Statistical method of determining the maximum response of building structure during an earthquake, in: Proc. Of the 2nd WCEE, vol. 2, 1960, pp. 781–798.
[35] J. Li, J. Chen, Stochastic Dynamics of Structures, Wiley, New York, 2009.
[36] A. McKane, H. Luckock, A. Bray, Path integrals and non-Markov processes. I. General Formalism, Phys. Rev. A 41 (2) (1990) 644.
[37] S. Einchcomb, A. McKane, Use of Hamiltonian mechanics in systems driven by colored noise, Phys. Rev. 51 (4) (1995) 2974.
[38] S. Machlup, L. Onsager, Fluctuations and irreversible process. II. Systems with kinetic energy, Phys. Rev. 91 (6) (1953) 1512.
[39] H.S. Wio, P. Colet, M. San Miguel, L. Pesquera, M. Rodriguez, Path-integral formulation for stochastic processes driven by colored noise, Phys. Rev. 40 (12) (1989) 7312.
[40] P. Colet, H.S. Wio, M. San Miguel, Colored noise: a perspective from a path–integral formalism, Phys. Rev. 39 (11) (1989) 6094.
[41] P. Hänggi, Path integral solutions for non–Markovian processes, Z. Phys. B Condens. Matter 75 (2) (1989) 275–281.
[42] T. Newman, A. Bray, A. McKane, Inertial effects on the escape rate of a particle driven by colored noise: an instanton approach, J. Stat. Phys. 59 (1) (1990) 357–369.
[43] A.N. Drozdov, P. Talkner, Path integrals for Fokker–Planck dynamics with singular diffusion: accurate factorization for the time evolution operator, J. Chem. Phys. 109 (6) (1998) 2080–2091.
[44] J. Donoso, J. Salgado, M. Soler, Short–time propagators for nonlinear Fokker–Planck equations, J. Phys. Math. Gen. 32 (20) (1999) 3681.
[45] H.S. Wio, Path Integrals for Stochastic Processes: an Introduction, World Scientific, 2013.
[46] G.M. Ewing, Calculus of Variations with Applications, Dover, New York, 1985.
[47] R.P. Agarwal, D. O'Regan, Ordinary and Partial Differential Equations: with Special Functions, Fourier Series, and Boundary Value Problems, Springer Science & Business Media, 2008.
[48] L.F. Shampine, I. Gladwell, S. Thompson, Solving ODEs with Matlab, Cambridge University Press, 2003.
[49] A.H.-S. Ang, W.H. Tang, Probability Concepts in Engineering Planning and Design: Emphasis on Application to Civil and Environmental Engineering, Wiley, New York, 2007.
[50] W.J. Pierson, L. Moskowitz, A proposed spectral form for fully developed wind seas based on the similarity theory of S.A. Kitaigorodskii, J. Geophys. Res. 69 (24) (1964) 5181–5190.
[51] K. Hasselmann, T.P. Barnett, E. Bouws, H. Carlson, D.E. Cartwright, K. Eake, J.A. Euring, A. Gicnapp, D.E. Hasselmann, P. Kruseman, A. Meerburg, P. Mullen, D.J. Olbers, K. Richren, W. Sell, H. Walden, Measurements of wind-wave growth and swell decay during the joint North Sea wave project (JONSWAP), Ergänzungsheft zur Deutschen Hydrographischen Zeitschrift A 8 (1973) 1–95.
[52] M. Shinozuka, G. Deodatis, Simulation of stochastic processes by spectral representation, Appl. Mech. Rev. 44 (4) (1991) 191–204.
[53] J. Liang, S.R. Chaudhuri, M. Shinozuka, Simulation of nonstationary stochastic processes by spectral representation, J. Eng. Mech. 133 (6) (2007) 616–627.
[54] J. Morison, J. Johnson, S. Schaaf, et al., The force exerted by surface waves on piles, J. Petrol. Technol. 2 (05) (1950) 149–154.
[55] M. Kim, A. Tahar, Y. Kim, et al., Variability of TLP motion analysis against various design methodologies/parameters, in: The Eleventh International Offshore and Polar Engineering Conference, International Society of Offshore and Polar Engineers, 2001.
[56] A. Naess, O. Gaidai, S. Haver, Efficient estimation of extreme response of drag-dominated offshore structures by Monte Carlo simulation, Ocean Eng. 34 (16) (2007) 2188–2197.
[57] P.D. Spanos, R. Ghosh, L.D. Finn, J. Halkyard, Coupled analysis of a spar structure: Monte Carlo and statistical linearization solutions, J. Offshore Mech. Arctic Eng. 127 (1) (2005) 11–16.
[58] P.D. Spanos, T.W. Chen, Random response to flow-induced forces, J. Eng. Mech. Div. 107 (6) (1981) 1173–1190.
[59] M. Shinozuka, Structural response variability, J. Eng. Mech. 113 (6) (1987) 825–842.
[60] B. Øksendal, Stochastic Differential Equations, Springer-Verlag, Berlin, 2003.